THE TOPOLOGY OF MAGNETIC RECONNECTION IN SOLAR FLARES

by

Angela Colman Des Jardins

A dissertation submitted in partial fulfillment
of the requirements for the degree

of

Doctor of Philosophy

in

Physics

MONTANA STATE UNIVERSITY
Bozeman, Montana

JULY 2007

APPROVAL

of a dissertation submitted by

Angela Colman Des Jardins

This dissertation has been read by each member of the dissertation committee and has been found to be satisfactory regarding content, English usage, format, citations, bibliographic style, and consistency, and is ready for submission to the Division of Graduate Education.

Dr. Richard Canfield

Approved for the Department of Physics

Dr. Bill Hiscock

Approved for the Division of Graduate Education

Dr. Carl A. Fox, Vice Provost

STATEMENT OF PERMISSION TO USE

In presenting this dissertation in partial fulfillment of the requirements for a doctoral degree at Montana State University, I agree that the Library shall make it available to borrowers under rules of the Library. I further agree that copying of this dissertation is allowable only for scholarly purpose, consistent with "fair use" as prescribed in the U.S. Copyright Law. Requests for extensive copying or reproduction of this dissertation should be referred to Bell & Howell Information and Learning, 300 North Zeeb Road, Ann Arbor, Michigan 48106, to whom I have granted "the exclusive right to reproduce and distribute my dissertation in and from microform along with the non-exclusive right to reproduce and distribute my abstract in any format in whole or in part."

Angela Colman Des Jardins

JULY 2007

To Liebe -
I’m the lucky one

ACKNOWLEDGMENTS

I would like to extend great thanks to: my committee, especially Dick and Dana, for many years of good advice and support; all of the people in physics department at MSU who bend over backwards to help the graduate students; the RHESSI teams at GSFC and UC Berkeley for their assistance with data analysis and the financial support; my family and friends for being there through exciting research results as well as health issues and for understanding that I'm not studying astrology.

Specific thanks to the people who gave their moral support: Sam - you're the only one who really knows what it took; Jaime Ahlberg, Jennifer Chase and Tina Ford for always knowing what to say; Mom for putting me on a pedestal; my workout partners Joey Key and Sytil Murphy for listening to the day-to-day issues; Dad for pointing me in the right direction when I was four; Julie Des Jardins for great conversations and the connection to normalcy; Diane Des Jardins for many home-cooked meals and unwavering kindness; Trae Winter for saving my sanity when it came to computer issues and for making traveling and sharing an office fun; and finally Io and Quark for distracting me from time to time and Cygnus for not eating this dissertation.

TABLE OF CONTENTS

LIST OF TABLES

LIST OF FIGURES

ABSTRACT

In order to better understand the location and evolution of magnetic reconnection, which is thought to be the energy release mechanism in solar flares, I combine the analysis of hard X-ray (HXR) sources observed by RHESSI with a three-dimensional, quantitative magnetic charge topology (MCT) model.

I first examine the evolution of reconnection by analyzing the relationship between observed HXR footpoint motions and a topological feature called spine lines. With a high degree of confidence, I find that the HXR footpoints sources moved along the spine lines. The standard two dimensional flare model cannot explain this relationship. Therefore, I present a three dimensional model in which the movement of footpoints along spine lines *can* be understood.

To better analyze the location of reconnection, I developed a more detailed method for representing photospheric magnetic fields in the MCT model. This new method can portray internal changes and rotations of photospheric magnetic flux regions, which was not possible with the original method.

I then examine the location of reconnection by assuming a relationship between the build-up of energy in stressed coronal magnetic fields and the measurement of the change in separator flux per unit length. I find that the value of this quantity is larger on the separators that connect the HXR footpoint sources than the value on the separators that do not. Therefore, I conclude that we are able to understand the location of HXR sources observed in flares in terms of a physical and mathematical model of the topology of the active region.

In summary, based on the success of the MCT model in relating the motion of HXR sources to the evolution of magnetic reconnection on coronal separators, as well as my mathematical and physical model of energy storage at separators, I conclude the MCT model gives useful insight into the relationship between sites of HXR emission and the topology of flare productive active regions.

CHAPTER 1

INTRODUCTION

Motivation

The first solar flare was observed independently by R. C. Carrington and R. Hodgson on 1 September 1859. Both Carrington and Hodgson were observing sun spots in white light when they saw an intense brightening near a complex spot group. We now know that only the most energetic solar flares produce the type of white light emission they observed that day. Solar flares result from rapid release of energy in the solar corona and are typically observed as enhancements in the emission of a wide range of wavelengths including radio, Balmer-α emission of neutral hydrogen – called Hα, ultra violet (UV), extreme ultra violet (EUV), soft X-rays (SXR) and hard X-rays (HXR). Since we are unable to view the Sun from Earth in many of these wavelengths, our knowledge of solar flares was limited until the advent of spacecraft in the 1960's. While our observational and theoretical understanding of flares has advanced greatly since 1859, there are still several scientific questions about flares, including how a vast amount of energy is stored over tens of hours and how it is released in tens of minutes.

The intensity and energy output of solar flares varies greatly. The strength of a solar flare is commonly given by its flux in 1-8 Å soft X-rays at 1 AU, where a C flare has a flux on the order of 10^{-3}*erg* $cm^{-2}s^{-1}$. Some flares are so weak that they are on the edge of detection by current soft X-ray telescopes. Others are so powerful that their soft X-ray flux is one (M flares), two (X flares), or even more orders of magnitude higher than C flares. The total amount of energy released during a solar flare in the form of thermal and nonthermal charged particles, kinetic energy and shock waves can exceed 10^{32} ergs.

The release of this large amount of energy has a variety of effects throughout the solar system. On Earth, solar flares can interact with our magnetic field and cause aurora as well as impact many man-made systems such as radio communication, navigation, satellites, aircraft, power grids and pipelines. As a recent example, nearly half of the satellites that comprise the Global Positioning System (GPS), used in a wide range of important navigation systems, were temporarily shut down as the result of a solar flare in December of 2006.

In order to reduce the negative effects on such of systems, we need a way to predict where and when solar flares will occur. The accurate prediction of flares is likely years in the future, but the more we are able to comprehend the physical nature of flares, the closer we will come to this goal. While it is now commonly accepted that solar flares are driven by the release of energy stored in magnetic field configurations, our theoretical understanding of *how* this energy is stored and released is far from comprehensive. In this dissertation, I complete a detailed analysis of flaring active region magnetic fields in an effort to further our insight into this scientific question.

Flare Energy Release

An example of a typical large flare is the M5 flare that occurred on 4 November, 2004. Figure 1.1 shows two light curves of this flare, one in the 6-12 keV (SXR) energy band and one in the 25-50 keV (HXR) band. These light curves were generated from data taken by the Ramaty High-Energy Solar Spectroscopic Imager (RHESSI *Lin et al.*, 2002), which observes the Sun in HXR and gamma-rays. While both the light curves rise at approximately the same time, the 25-50 keV band peaks prior to the 6-12 keV band. This lag in SXR emission, known as the Neupert effect (*Neupert*, 1968; *Hudson*, 1991), is due to the physical process that transfers the energy of flare accelerated nonthermal electrons into heating. In the thick-target bremsstrahlung model, where, due to collisions, the spectrum of

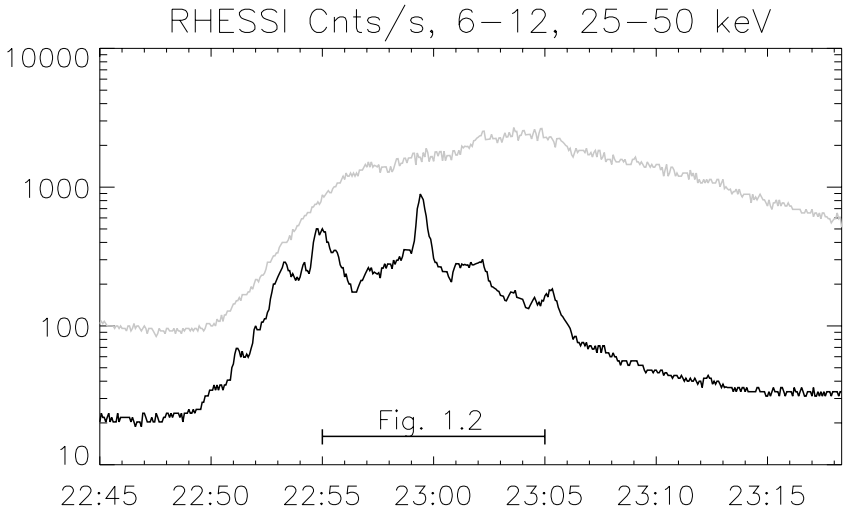

Figure 1.1: RHESSI light curves from a M5 flare on 4 November, 2004. The grey/black curves are the counts per second in the 6-12 keV/25-50 keV energy ranges, respectively.

a population of particles changes as it passes through the target, the HXR emission peaks when most of the nonthermal electrons hit the chromosphere and cause impulsive heating. A consequence of this heating is an increase in the local pressure, which causes chromospheric plasma to evaporate into the corona, where it is observed in the form of SXR and EUV emissions.

The first phase of a flare is called the impulsive phase, because over this time period, which generally lasts for a few minutes, the HXR, radio and EUV emissions have a spikey, impulsive profile (see black curve in Figure 1.1). After the peak of the impulsive phase, the SXR and Hα emissions may continue to increase for 10-20 minutes before they gradually decay for as long as several hours (see grey curve in Figure 1.1). Based on spectroscopic observations taken over the past few decades, the spikey structure observed in HXR during the impulsive phase is typically attributed to nonthermal emission and the smooth SXR curve is attributed to thermal emission.

With the RHESSI telescope, we can observe both SXR and HXR as well as use spec-

troscopy to determine the thermal and nonthermal features of a flare. Figure 1.2 shows a RHESSI count flux spectra (counts $cm^{-2}s^{-1}keV^{-1}$) of the impulsive phase (~22:55-23:05) of the 4 November 2004. The 3 to 20 keV range of the spectrum is dominated by thermal (blackbody) radiation. This SXR/HXR emission has a temperature of 10 to 20 MK and is emitted by hot plasma that fills the flare loop. Due to the strong magnetic field and the low thermal pressure, the shape of flare loops are determined by the shape of the loop's magnetic field lines. Other thermal emission is observed in the chromosphere (Hα and UV) at the base of flare loops and in the corona (EUV) in cooler, ~1 MK post flare loops.

Above 20-30 keV, flare spectra are dominated by nonthermal emission, which can be characterized by a power-law. Nonthermal emission is typically observed in HXR, UV and Hα at the base of flare loops (footpoint sources).

In some flares, especially large flares associated with coronal mass ejections (CMEs), the brightening in Hα and UV is not concentrated in a single source, but has two extended sources, or ribbons, that separate as the flare progresses. In an effort to explain this commonly observed phenomenon in terms of the physical mechanism that releases the energy stored in flaring active region magnetic fields, the CSHKP model (*Carmichael*, 1964; *Sturrock*, 1968; *Hirayama*, 1974; *Kopp and Pneuman*, 1976), now refered to as the standard model of solar flares, was developed.

The CSHKP model, shown in Figure 1.3, is a 2D model that describes how stressed magnetic field lines are pushed together such that they form a current sheet at the X-point, where field lines from the sides of the configuration are *reconnected* (see e.g. *Priest and Forbes*, 2000) to form new field lines above (open) and below (closed) the reconnection region. In the CSHKP model, the reconnection region is refered to as an X-point because this is the shape made by the intersection of the separatrix surfaces in 2D. A separatrix is a surface that divides magnetic field lines into regions of different connectivity.

Magnetic reconnection is commonly accepted as the way stressed coronal magnetic

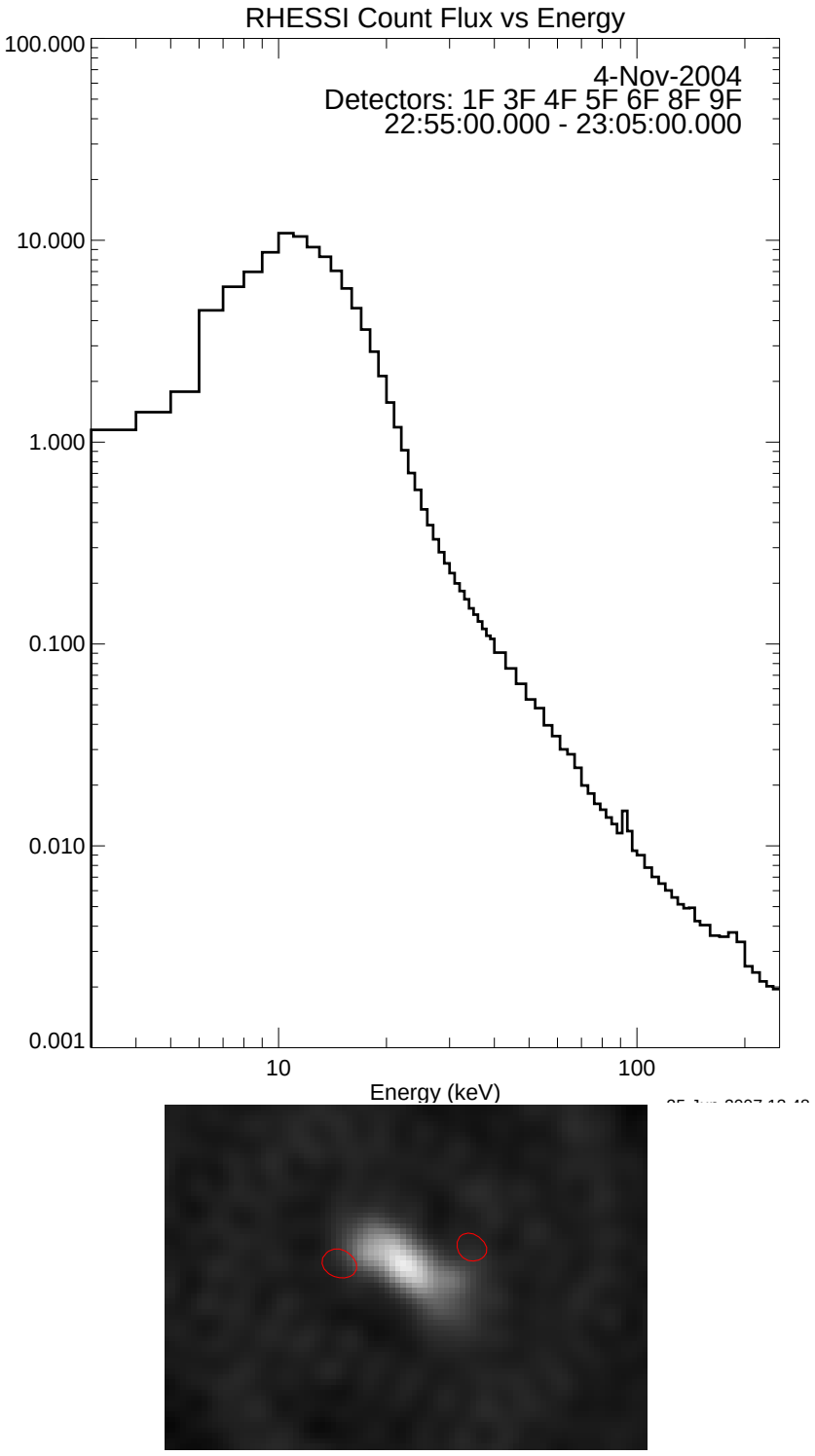

Figure 1.2: Top: RHESSI spectrum (in counts $cm^{-2}s^{-1}keV^{-1}$) from the impulsive phase (22:55 - 23:05 UT) of the 4 November 2004 flare. Bottom: RHESSI 6-12 keV image with 25-50 keV contours (drawn at 70% of the maximum) summed over the same time period as the spectrum.

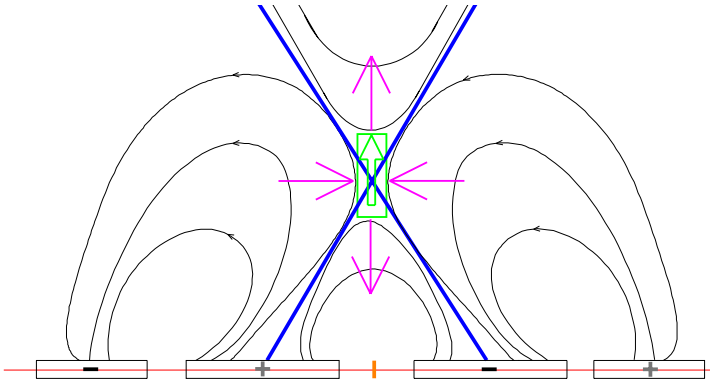

Figure 1.3: Diagram of the CSHKP model. The red line is the photospheric surface, the black lines are example field lines, the blue lines indicate separatrix surfaces, the orange dash a polarity inversion line, and the green box is the reconnection region. Purple arrows show the direction the field lines are pushed and the green arrow shows the direction of the reconnection region as the flare progresses.

fields undergo topological change to restructure and release free energy. Reconnection processes can occur in a slow, steady way but more often happen as sudden violent events manifested as flares and CMEs. During reconnection, particles are accelerated, shock waves are formed and plasma is heated. The particles accelerated in this process stream along magnetic field lines close to the reconnection region until they bombard the chromosphere, which results in both thermal and nonthermal emission, exhibited in Figures 1.1 and 1.2.

As the process of reconnection continues in the CSHKP model, the reconnection region moves higher into the corona as more and more closed field lines are piled up under the X-point. A consequence of the upward 'movement' of the X-point and the fact that the coronal field lines are line-tied to the lower atmosphere is the 'movement' of the Hα flare ribbons away from the polarity inversion line (PIL), which divides regions of opposite magnetic polarity on the photosphere. The chromospheric material composing the ribbons does not actually move, but rather the ribbons shift due to the changing locations of heating and

excitation in the chromosphere.

The same is true for the 'motion' of HXR footpoint sources, which are considered to be more directly associated with the production of high energy electrons in the reconnection region than Hα or UV sources. HXR are less ambiguous than Hα and UV observations because the latter can also be caused by thermal emission and require less energy deposition to generate. Recently, much interest has surrounded flares that exhibit moving HXR footpoint sources because most HXR sources do not follow the same simple expansion away from the PIL as the Hα ribbons.

Although we have observational evidence for the particle acceleration that is thought to accelerate the electrons responsible for this bursty HXR emission as well as accelerate protons and nuclei, the sources of the accelerating electric fields are still not understood. One possibility is the DC electric field generated in current sheets or during fast reconnection. Numerical simulations indicate that this field could produce electron accelerations up to about 100 keV before the electrons are scattered out of the reconnection region (*Foukal*, 2004).

Another acceleration mechanism is 'stochastic' acceleration by turbulence and waves. Here, particles are reflected from scattering centers that, on average, impart energy to the particle. Stochastic acceleration can operate over a much larger region and produce the double HXR footpoints. The main weakness of this mechanism is that the required energy spectrum of waves and turbulence is unknown (*Foukal*, 2004).

While the CSHKP model describes the observed expansion of Hα/UV ribbons, it fails to predict the motion of HXR footpoint sources. In this model, HXR sources are predicted to follow the same increasing separation away from the PIL as the thermal flare ribbons. In reality, only a small percentage of observed HXR footpoint sources exhibit this type of motion. Often, HXR sources are observed to move parallel to the PIL, either away from, towards, or nearly parallel to one another. These types of motion cannot be explained by

this 2D standard flare model. Also, the footpoint separation velocity predicted in the standard model is a only few km s^{-1}(*Somov et al.*, 1998). Actual observed apparent velocities are much larger, on the order of 50 km s^{-1}. To account for the observed directions and speeds of HXR footpoint sources, and thus the evolution of reconnection, a 3D model is needed.

Flare Energy Storage

After the standard model for the release of energy in a solar flare was developed, the next question became how so much energy is made available to fuel a flare. Current evidence points to the build-up of energy over days as the photospheric magnetic field shifts continuously prior to a flare. Changes in the field at the photospheric boundary (almost certainly driven by sub-photospheric phenomona) drive the chromospheric and coronal plasma. The coronal field may remain nearly potential (current-free), but accumulates a non-potential component related to current layers that separate interacting magnetic fluxes and thus prevent coronal flux changes (*Henoux and Somov*, 1987). In other words, energy is stored in the corona due to changes in the photospheric boundary because no reconnection takes place and the magnetic configuration becomes stressed. The field becomes more and more non-potential until some critical point is reached and a flare occurs.

Past research on energy storage prior to a flare has concentrated on non-potential signatures in the photospheric fields as observed by vector magnetograms (i.e. *Gary et al.*, 1987; *Wang et al.*, 1996; *Moon et al.*, 2000; *Deng et al.*, 2001; *Tian et al.*, 2002; *Falconer et al.*, 2006; *Dun et al.*, 2007). These yield maps of not only the magnitude of the field but also the its direction. For example, *Dun et al.* (2007) calculated the daily average values of three non-potential parameters from vector magnetograms of selected regions along the main neutral lines of active region 10486. They found that the three non-potentiality parameters increased at the impulsively brightening flare sites from values measured at least

one day before the two large X-class flares of 28 and 29 October, 2003. While most of the measured parameters decreased after the flares, as expected due to the relaxation of non-potentiality, some continued to increase. This and other, similar studies indicate that more research is required to fully understand the relationship between observational signatures of nonptentiality and the build-up and release of energy in flaring active regions.

The CSHKP model is useful for explaining energy release in a simple two dimensional configuration, but it does not give us any information on how or where the coronal field becomes stressed. Also, while the studies of non-potential fields from photospheric vector magnetograms cited above significantly advance our understanding of energy storage, these studies do not deal with coronal fields. A fully three dimensional topology model that defines the locations of energy storage and release is needed.

Observations and Analysis

Hard X-ray Images

The RHESSI telescope observes solar X-rays and gamma-rays from 3 keV to 17 MeV with energy resolution of ~1 keV, time resolution of ~2 s and spatial resolution as high as $2.3''$. Instead of focusing optics, imaging is based on rotating modulation collimators that time-modulate the incident flux as spacecraft rotation causes the field of view of the collimators to sweep across the Sun. Ground based software then uses the modulated signals to reconstruct images of HXR sources (*Hurford et al.*, 2002).

The RHESSI telescope consists of a set of nine bi-grid subcollimators, each consisting of a pair of widely separated grids in front of a corresponding non-imaging detector. Each grid consists of an array of equally-spaced, X-ray-opaque slats separated by transparent slits. Within each subcollimator, the slits of the two grids are parallel and their pitches are identical. The transmission through the grid pair depends on the direction of the incident X-rays. If the direction of incidence is changed as a function of time, the transmission of

the grid pair is modulated in time as the shadow of the slats in the top grid alternately falls on the slits or slats in the rear grid. This modulation is achieved by rotating the spacecraft at 15 revolutions per minute.

Due to the temporal and spectral resolution of the detectors and the fact that RHESSI is a collimator-based Fourier-transform imager rather than a direct imager, RHESSI HXR images can be reconstructed in a wide variety of energy and time bins. This powerful ability enables the detailed examination of the temporal, spatial and spectroscopic behavior of flares. Most importantly, RHESSI observations allow for the determination of the location and evolution of HXR footpoints, which when combined with a quantitative topology model, can be related to the location and evolution of magnetic reconnection.

Topology

In order to understand the topological location of magnetic reconnection, the connectivity of the magnetic field needs to be characterized in 3D. This connectivity (topology) is determined by using a Magnetic Charge Topology (MCT) model where magnetic point charges represent regions of strong magnetic flux at the photospheric boundary. The calculation of the topology begins by selecting a subregion, namely the main body of the active region, from full-disk Solar and Heliospheric Observatory/Michelson Doppler Imager (SOHO/MDI; *Scherrer et al.*, 1995) line-of-sight magnetograms. Next, the observed field is partitioned into strong-field regions by grouping pixels that exceed a set threshold and are downhill from the local maximum. Each region is then replaced by a point source which matches the region's net flux and is located at the region's centroid. These point sources, or *poles*, form the photospheric boundary of the topology calculation and thus their relative locations and strengths define all other topological features.

Figure 1.4 shows several topological features that are important to reconnection in flares. *Poles* are the positive and negative point sources of magnetic flux, an idealization

of well-defined features like sun spots and pores. The set of all field lines originating at a given positive pole and ending at a given negative pole fills a volume of space called a *domain*. A *separatrix* is a boundary surface dividing domains.

Null points are the locations where the magnetic field vanishes. Near null points, the magnetic field is approximately

$$\boldsymbol{B}(\boldsymbol{x}_a + \delta\boldsymbol{x}) \approx \mathbf{J}^a \cdot \delta\boldsymbol{x}, \tag{1.1}$$

where $J^a_{ij} = \partial B_i/\partial x_j$ is the Jacobian matrix evaluated at x_a. This matrix has three eigenvalues which sum to zero because it must be traceless; $\boldsymbol{\nabla} \cdot \boldsymbol{B} = 0$. If two eigenvalues are positive (negative) then the null is positive (negative). The eigenvectors associated with the two like-signed eigenvalues define the *fan*, in which the separatrix field lines lie. The third eigenvector defines one parallel and one anti-parallel *spine* field line, which connect the null's two spine poles. A spine line usually lies in the photosphere, extending from a pole through a null to another pole of the same polarity. A *separator* field line, which starts and terminates at null points, is the intersection between separatrix surfaces. Separators are the generalization to three dimensions of two-dimensional X-points and are hypothesized to be the main locations for reconnection in MCT models (*Greene*, 1988; *Lau and Finn*, 1990).

Previous studies of the topology of flaring configurations have related features such as separators, separatricies and quasi-separatrix layers (QSLs; regions of drastic change in field-line linkage) to various types of flare emission. *Henoux and Somov* (1987) developed a theory that reconnection along one main separator interrupts currents flowing along lines of force, releasing energy stored in the currents. *Gorbachev and Somov* (1988, 1989) applied this theory to an observed flare, showing that field lines passing close to the separator connect to the chromospheric flare ribbons. In order to represent the photospheric field in a more realistic way, the source method, which has many sources and separatricies, was

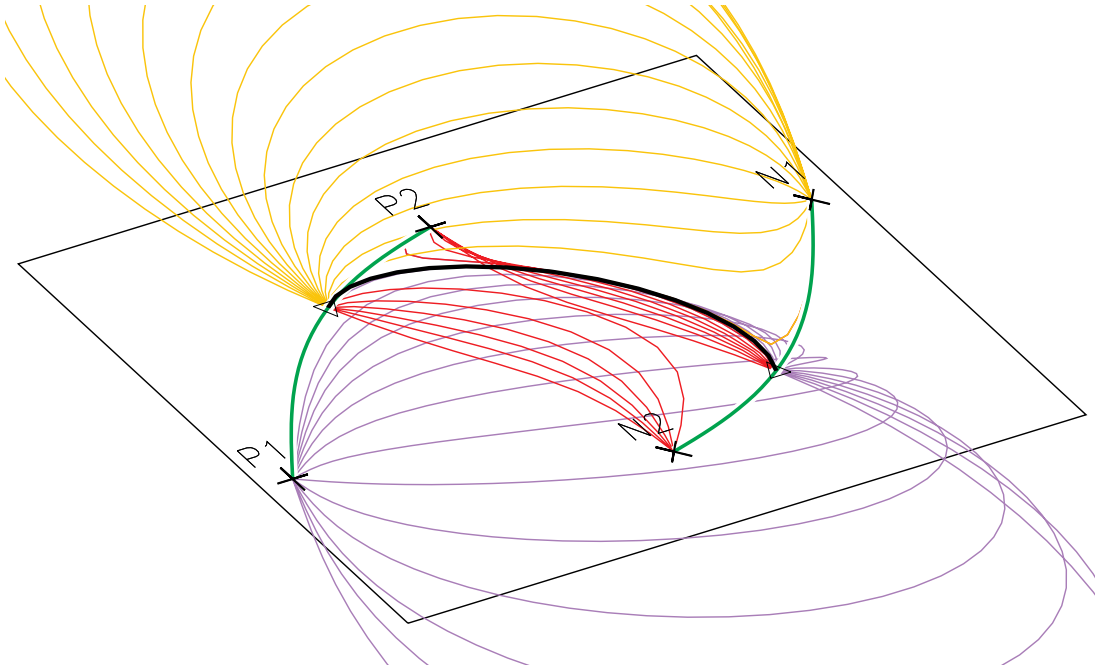

Figure 1.4: Quadrupolar diagram with key topological features. P2 and P1 (+) are are positive poles while N1 and N2 are negative poles ($\times$). The triangles are null points, one positive ($\bigtriangledown$) and one negative ($\bigtriangleup$). The orange, purple and red field lines lie on the separatrix surface under which exist all of the field lines connecting P2/N1, P1/N2 and P2/N2 respectively. Above the orange and purple separatricies is the domain containing all of the field lines that connect P1 to N1. All four of these domains intersect at the separator (thick black line). The thick green lines are the spine lines.

introduced (i.e. *Titov et al.*, 2003; *Demoulin et al.*, 1994; *Bagala et al.*, 1995; *Wang et al.*, 2002). Analyses of flares using both the source method and QSLs have shown that Hα and UV flare brightenings are located along the intersections of separatricies (source method) or QSLs with the chromosphere (*Mandrini et al.*, 1991; *Demoulin et al.*, 1994; *Bagala et al.*, 1995; *Aulanier et al.*, 1998; *Lee et al.*, 2003; *Demoulin et al.*, 1997; *Wang et al.*, 2000). These results strongly suggest that the location of energy release in flares is defined by the magnetic topology (*Démoulin*, 2006).

One might use QSLs or the source method to examine the topological location of magnetic reconnection, but the use of a magnetic charge topology (MCT) model with point sources located on the photospheric surface has several advantages. These include: 1) Powerful mathematical tools can be used because the topological features are quantitatively defined. This includes the ability to calculate the spine lines associated with the field and to calculate the magnetic flux linked by separators, both of which are employed in this dissertation. 2) Model sources represent the fluxes and locations of strong photospheric fields, thus the photospheric boundary of the model is a quantitative representation of the observed line of sight magnetogram. 3) Calculation of the topological features of the model coronal field is not computationally time consuming, so we are able to study several cases.

Overview

In this dissertation, I take the next step in the analysis of flare energy storage and release by combining HXR observations with a 3D quantitative model of the flaring active region's topology. To do this, I use the following working hypothesis: In the absence of major reconnection, coronal magnetic fields become stressed as the photospheric boundary slowly evolves due to the emergence of new field and horizontal flows. When a critical point is reached, this energy is released by the rapid reconnection of magnetic field lines near the separator. As a result, electrons are accelerated near the reconnection region and stream

along field lines near the separator. Upon encountering the chromosphere, the electrons undergo bremsstrahlung and non-thermal HXR are emitted. Thus, I interpret HXR footpoint sources as the location of the chromospheric ends of newly reconnected field lines, which lie close to the separator.

In Chapter 2, I examine the evolution of the reconnection that releases free magnetic energy by proposing a model for how the change of separators during a flare can result in HXR source motions. In Chapter 3, I describe a new technique for representing photospheric magnetic fields in topology calculations. In Chapter 4, I examine the location of reconnection by relating the storage of energy to changes in separators. Finally, in Chapter 5, I summarize the conclusions I reach by combining my studies of reconnection evolution and location.

Chapter 2, 'Reconnection in Three Dimensions: the Role of Spines in Three Eruptive Flares' (*Des Jardins et al.*, 2007a), and Chapter 4, 'Signatures of Magnetic Stress Prior to Three Flares Observed by RHESSI' (*Des Jardins et al.*, 2007b), are papers that have been submited for publication in the Astrophysical Journal. As of July, 2007, Chapter 4 has been accepted and Chapter 2 is still in the referee review process.

CHAPTER 2

RECONNECTION IN THREE DIMENSIONS: THE ROLE OF SPINES IN THREE ERUPTIVE FLARES

Abstract

In order to better understand magnetic reconnection and particle acceleration in solar flares, we compare the RHESSI hard X-ray (HXR) footpoint motions of three flares with a detailed study of the corresponding topology given by a Magnetic Charge Topology (MCT) model. We analyze the relationship between the footpoint motions and a topological feature called spine lines and find that the examined footpoints sources moved along the spine lines. HXR footpoint motions predicted by the standard 2.5D flare model *cannot* explain this relationship. We present a 3D model in which the movement of footpoints along spine lines *can* be understood. Our 3D model also explains other important properties of HXR footpoint motions that cannot be described by the standard model, such as the sense of their relative motions.

Introduction

Magnetic reconnection is the mechanism of topological change that is thought to bring about energy release and non-thermal electron acceleration in solar flares. By studying the radiative output of flares in association with the magnetic topology of the flaring region, we can learn a great deal about the topological location of reconnection. Knowing the location of reconnection is key to understanding both flare trigger and evolution processes.

Since the wealth of data now available from Ramaty High Energy Solar Spectroscopic Imager (RHESSI; *Lin et al.*, 2002) exhibits many cases of hard X-ray (HXR) footpoint

motion, an explanation for the various types of movement is of great interest. For example, *Fletcher and Hudson* (2002) compare observed footpoint motions to those predicted by flare models. They conclude that footpoint motions do not resemble the simple increase in separation expected in 2D reconnection models. For the 29 October 2003 X10 flare, *Krucker et al.* (2005) analyze the HXR footpoint velocity variations and the underlying photospheric magnetic field strength. They observe that the footpoint velocity is generally slower in the areas where magnetic field strength is higher. *Bogachev et al.* (2005) analyze the HXR footpoint motions of 31 flares observed by the *Yohkoh* Hard X-ray Telescope (HXT; *Kosugi et al.*, 1991) with respect to neutral lines calculated from photospheric magnetograms. They find that only 13% of footpoints move away from the neutral line.

Several groups have sought to explain flare features via topological models. *Gorbachev and Somov* (1988) describe a topological model which satisfies the observational requirements of two-ribbon flares, such as HXR 'knots' in the ribbons. In their model, the active region separator, the special field line on which reconnection occurs, directs the released energy flux to the flare ribbons. *Somov et al.* (1998) present a reconnection model which explains the observation that the separation of HXR footpoints in 'less impulsive' flares (impulsive phase $t >$ 30-40 s) tends to increase while in 'more impulsive' flares ($t <$ 30-40 s), it decreases. They attribute the increase/decrease in footpoint separation to an increase/decrease in the longitudinal field at the flaring separator, increasing/decreasing the length of the reconnected field lines.

While substantial work has been done in the areas of multi-wavelength analysis of solar flares and coronal magnetic field modeling, little attention has been given to the combination of these two fields. *Metcalf et al.* (2003) describe a coincidence between magnetic separatricies and features of the 25 August 2001 white-light flare. They conclude that the HXR footpoint motions present in this flare are consistent with reconnection at a separator. Here, we explore three flares by examining the relationship between HXR footpoints and

spine lines.

In this Chapter, for the first time, we compare flare HXR footpoint motions observed by RHESSI and a detailed study of the active region's magnetic topology. This examination is conducted using data from the Solar and Heliospheric Observatory's Michelson Doppler Imager (SOHO/MDI; *Scherrer et al.*, 1995) and a magnetic charge topology model (MCT; see *Longcope*, 2005). The MCT model allows us to observationally characterize the connectivity of coronal field lines by defining distinct source regions in the photosphere. We use this information to explain footpoint motions within the framework of magnetic reconnection – the transport of flux from one pair of sources to another – and flare models.

Several topological features are important to reconnection in flares (for terminology see *Longcope*, 2005). *Poles* are the positive and negative point sources of magnetic flux, an idealization of well-defined features like sun spots and pores. The set of all field lines originating at a given positive pole and ending at a given negative pole fills a volume of space called a *domain*. A *separatrix* is a boundary surface dividing domains. *Null points* are the locations where the magnetic field vanishes. Near null points, the magnetic field is approximately

$$\boldsymbol{B}(\boldsymbol{x}_a + \delta\boldsymbol{x}) \approx \mathbf{J}^a \cdot \delta\boldsymbol{x}, \tag{2.1}$$

where $J^a_{ij} = \partial B_i/\partial x_j$ is the Jacobian matrix evaluated at x_a. This matrix has three eigenvalues which sum to zero because it must be traceless; $\boldsymbol{\nabla} \cdot \boldsymbol{B} = 0$. If two eigenvalues are positive (negative) then the null is positive (negative). The eigenvectors associated with the two like-signed eigenvalues define the *fan*, in which the separatrix field lines lie. The third eigenvector defines one parallel and one anti-parallel *spine* field line, which connect the null's two *spine poles*. A spine line usually lies in the photosphere, extending from a pole through a null to another pole of the same polarity. A *separator* field line, which starts and terminates at null points, is the intersection between separatrix surfaces. A separator is the

generalization to three dimensions of a two-dimensional X-point. While reconnection can also occur on separatrix surfaces, separators are hypothesized to be the main location for reconnection in MCT models (*Greene*, 1988; *Lau and Finn*, 1990).

There are several advantages to this MCT method including: 1) Due to the fact that the topological features are quantitatively defined, powerful mathematical tools can be used. One of these tools is the ability to calculate the spine lines associated with the field. 2) Model sources represent the fluxes and locations of strong photospheric fields, thus the photospheric boundary of the model is a quantitative representation of the observed line of sight magnetogram. Of course, we would like to apply a full nonlinear force-free field model to extrapolate the complex magnetic field of these flaring active regions into the corona. Such modeling, however, is beyond current computational capabilities at the level of complexity of the magnetic fields of the active regions we study below. 3) Calculation of the topological features of the model coronal field is not computationally time consuming, so we are able to study several cases. This is an advantage over models that use Quasi-Separatrix Layers (QSLs), whose intersections with the photosphere are analogous to spine lines, because the numerical techniques required to compute the coronal fields needed by QSL models are currently too limited (*Démoulin*, 2006).

In this Chapter, we present the analysis of three X class flares, each well observed by RHESSI, each exhibiting significant footpoint motion. We have examined the HXR emission in detail (see the Flare Observations and Analysis section), calculating the centroids of each footpoint source several times per minute, or as frequently as count statistics allowed. A MDI magnetogram close to each flare start time was used as an input to the MCT extrapolation model, resulting in a topological map of each flaring active region (see the Topology Observations and Analysis section). We then plotted the footpoint centroids on the topological maps and looked for a relationship between the spine lines and footpoint tracks. Details of this step is given in the Analysis of Footpoint Motions and Spine

Table 2.1: Flare properties. AR is the active region number and FP motion gives the time range over which the footpoints were observed to move.

Flare	Date	Location (heliocentric ″)	Peak Time (UT)	*GOES* Class	AR	FP Motion (UT)
A	29 Oct 2003	(100, -350)	20:48	X10	10486	20:41-20:57
B	7 Nov 2004	(330, 170)	16:06	X2	10696	16:21-16:30
C	15 Jan 2005	(150, 310)	22:50	X2	10720	22:34-22:58

Lines section. In the Discussion section, we propose a evolutionary model to answer two main questions raised by our observations. Firstly, why do the footpoints move along the spine lines? Secondly, does the standard flare model predict the direction and speed of the movement observed?

Flare Observations and Analysis

The criteria for the flares chosen in this study were that they occurred within 30 degrees of disk center, were well observed by RHESSI, and exhibited significant footpoint motion. Only a handful of flares fit these criteria, so while compact flares might have been a more simple starting place for this study, all three of the flares we examined were eruptive (as indicated by the Large Angle Spectroscopic Coronagraph (LASCO; *Brueckner et al.*, 1995) coronal mass ejection catalog). These flares occurred on 29 October 2003, 7 November 2004 and 15 January 2005, hereafter A, B and C respectively.

Flare A occurred on 29 October 2003, was observed by RHESSI during all but the decay phase and was one of several powerful flares unleashed by the complex active region 10486. Based on images from RHESSI and the Transition Region and Coronal Explorer (TRACE; *Handy et al.*, 1999), we conclude that this two-ribbon flare occurred in a sheared arcade of loops, a portion of which connected two HXR footpoints, shown with contours in Figure 2.1. Using the RHESSI software's image flux method on data summed over the front segments of all 9 detectors in the energy range 50-300 keV, we calculated the centroid of

the footpoint sources every 20s from when they first appeared at 20:41 UT until they faded out at 20:57 UT. The negative polarity footpoint (1N, top panel, Figure 2.2) moved steadily at $\sim$ 44 km s^{-1} along an extended region of negative flux with average field strength -650 G. The positive footpoint (1P) traveled at a slower rate ($\sim$ 18 km s^{-1}) through a large 1920 G positive source. From approximately 20:41-20:44 UT, a third footpoint source (2P) was present just below and to the east of source 1P. This source exhibited no significant motion during the short time it was observed. Footpoint 1N was present for the entire period while the weaker footpoint 1P was missing for two periods: 20:47:00-20:50:00 and 20:56:20-20:57:00 UT. A substantial decrease in count rate during the first of these periods (see 50-100 keV lightcurve in Figure 2.3) coincides with a decrease in flux of both footpoints, and footpoint 1P falls below the level of detection.

Flare B was recorded by RHESSI on 7 November 2004 from 16:05-17:04 UT with exception of a span between 16:32 and 16:45 UT. Flare B came right on the heels of an earlier thermal flare just to the west, which occurred mostly during RHESSI night. Both the negative (1N) and positive (1P) polarity footpoints (middle panel, Figure 2.2) are observed in each of a series of 10 s images from 16:20:50 to 16:30:00 UT. The images were made with the front segments of all 9 detectors in the energy range 25-300 keV. Footpoint 1N takes a curious path through a region with average line of sight field strength -680 G. For the first 2 minutes it moves to the west at $\sim$ 116 km s^{-1}, then travels for 3 minutes to the east before traveling again to the west at a slower rate ($\sim$ 58 km s^{-1}) about 5$''$ below the first westward movement. Footpoint 1P progresses at $\sim$ 80 km s^{-1} along an area of 500 G positive field for about 6 minutes, taking a sharp turn 2 minutes in before slowing down to $\sim$ 18 km s^{-1} in a stronger 1720 G source.

Flare C occurred on 15 January 2005 and was observed by RHESSI during its impulsive phase, from 22:15-23:15 UT. Two sets of footpoints were followed in a series of 20 s images using the front segments of all 9 detectors in the energy range 25-300 keV, starting

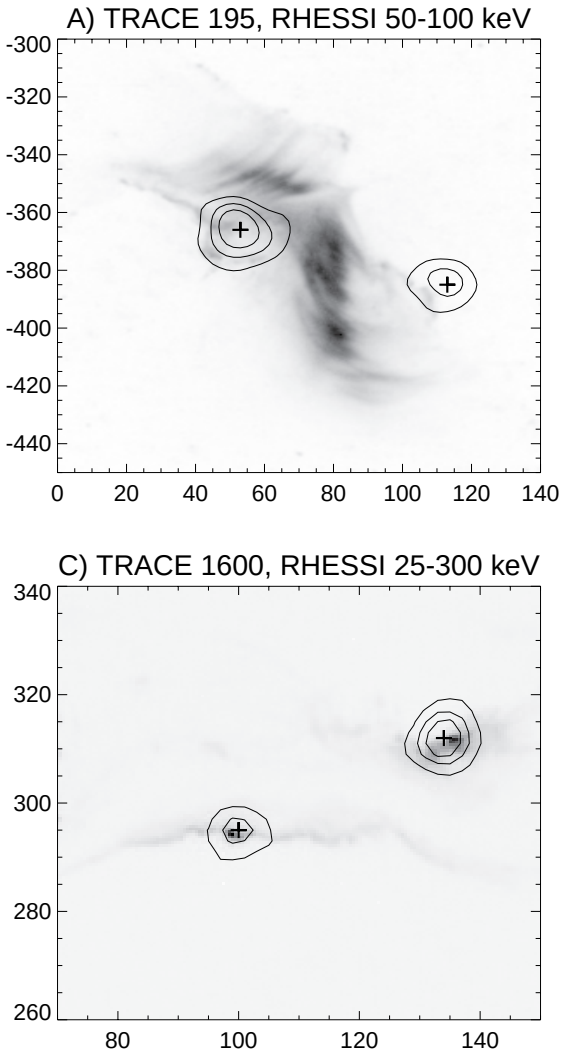

Figure 2.1: TRACE images from flares A and C with RHESSI contours. Top (flare A): TRACE 195 Å image with RHESSI 50-100 keV contours at 30, 50, 70% integrated for 4 s. Bottom (flare C): TRACE 1600 Å image with RHESSI 25-300 keV contours at 30, 50, 70% integrated for 20 s.

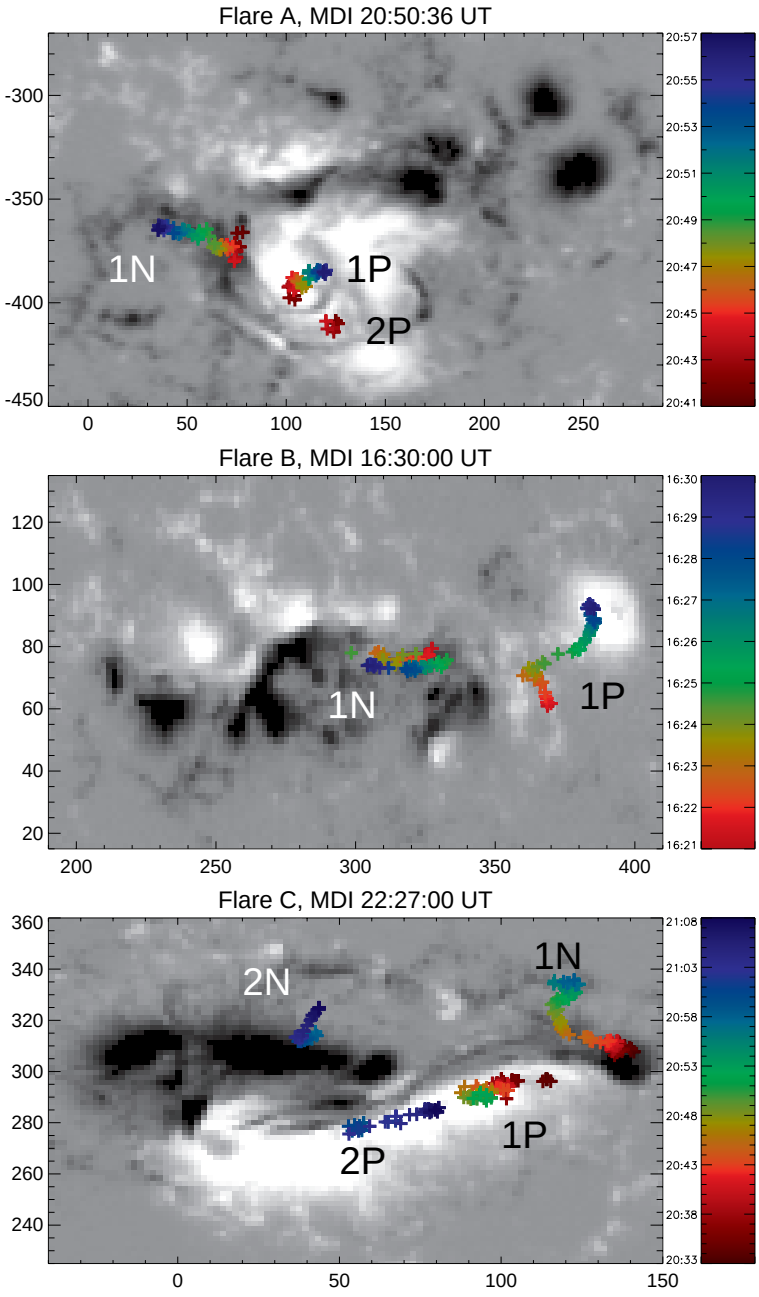

Figure 2.2: MDI line of sight magnetic field images of the three active regions (white is positive, black is negative) and RHESSI HXR footpoint tracks, which follow the color coded UT time scaling shown to the right. Each + symbol marks the centroid location of a source at 50-300, 25-300 and 25-300 keV for flares A, B and C respectively. The centroids are plotted with the following (UT) timing: A - every 20 s from 20:41:00-20:57:00, B - every 10 s from 16:20:50-16:30:00, C - every 20 s from 22:32:40-23:08:20.

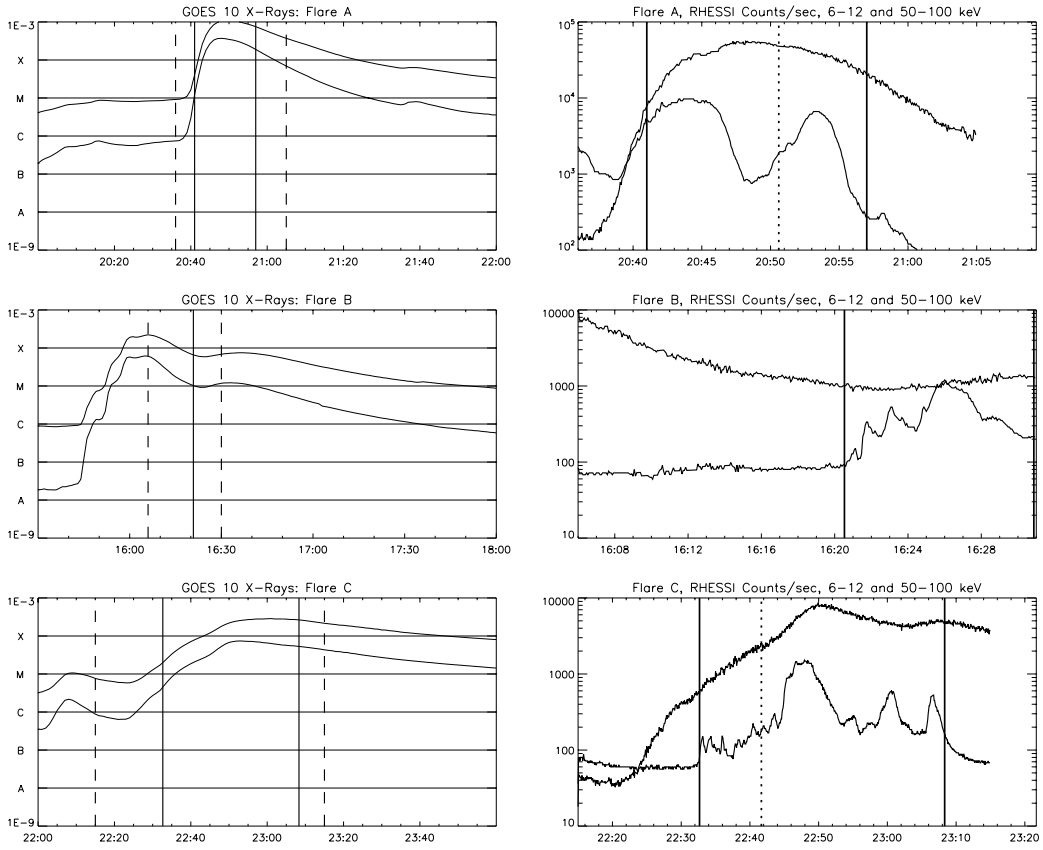

Figure 2.3: Left hand panels are GOES lightcurves for each flare. The dashed lines on the left panels indicate the time range for the right panels. Right hand panels are corrected count rates per second in the 6-12 (top) and 50-100 keV (bottom) energy bins for each flare. In both the right and left panels, the solid vertical lines indicate the time range over which the footpoint motion is observed and plotted in Figures 2.2 and 2.5. The dotted lines indicate the time of the images shown in Figure 2.1.

at 22:32:40 and continuing until 23:08:20 UT. The first set was observed from 22:32:40-22:59:00 UT, where the positive polarity footpoint (1P, bottom panel, Figure 2.2) disappears from the images after 22:53 UT. A second pair of footpoints (2P and 2N) was detected from 22:58:00-23:08:20 UT. Co-temporal TRACE 1600 Å images (Figure 2.1) show flare ribbons whose brightest parts are co-spatial with the first set of RHESSI footpoints (1P and 1N). The second set of footpoints was located to the west of the first, the positive polarity footpoint (2P) in the same region of positive flux as 1P, and the negative footpoint (2N) in a separate region from 1N. Footpoint 1P moved slowly ($\sim$ 12 km s^{-1}) through a region with average line of sight field strength 1770 G in a manner that was somewhat random but generally parallel to the nearby magnetic inversion line. Footpoint 1N progressed slowly ($\sim$ 14 km s^{-1}) out of a -1500 G region then moved more quickly ($\sim$ 46 km s^{-1}) through a -670 G area before jumping over to another -290 G source where it did a zigzag across about 10$''$ before RHESSI coverage was lost. The later set of footpoints, 2P and 2N, moved along a 1620 G extended source at $\sim$ 37 km s^{-1} and moved to the boundary of a -620 G region at $\sim$ 50 km s^{-1}, respectively. Due to its location, we hypothesize that the second set of footpoints was from a separate sympathetic flare. Further evidence for this hypothesis can be observed in the RHESSI lightcurves (Figure 2.3). At 22:58, when the second set of footpoints appears, the flux observed in the 6-12 keV energy band is decreasing, a sign that the first flare is decaying. However, the HXR emission (50-100 keV) continues for another 10 min and the 6-12 keV emission rises to a second peak. These factors led us to conclude that footpoints 2P and 2N were part of a sympathetic flare.

When discussing footpoint movements, one of the first steps to take is to establish footpoint conjugacy. We have done this using three techniques. First, we compare the general characteristics (e.g. start, peak and end times) of the HXR light curves of the candidate pair. If the two footpoints are connected by the same field lines, then the fast electrons running down either side of those lines should impact the chromosphere at approximately

the same time. With a 20 s imaging cadence, the sources' light curves should coincide. Second, we examine the MCT model topology to see if a connection exists between the positive and negative magnetic sources associated with the footpoints. Third, if an extreme ultraviolet image is available during the flare time, we look for a hot loop connecting the HXR source regions. This visual connection gives credence to hot evaporated plasma having filled up the newly reconnected loop. The employment of these techniques leads us to the conclusion that the HXR sources 1P and 1N of flare A are conjugate. Due to a lack of extreme ultraviolet images during flare B, the case for conjugacy is not as strong. However, the RHESSI data and topology lend enough support that we claim sources 1P and 1N of flare B are conjugate. Flare C has two sets of conjugate footpoints: sources 1P and 1N and sources 2P and 2N.

As a side note, we remark on an interesting observation involving the magnetic field strength associated with the HXR footpoint sources and the footpoint speeds. An anti-correlation between field strength and average footpoint speed was found to be significant at the 90% level via the calculation of the Kendall coefficient. The average speed of sources with underlying field strengths of less than 1000 G is ~ 59 km s^{-1} while the average speed for those with strengths of more than 1000 G is ~ 19 km s^{-1}. The relationship between field strength and footpoint speed has been noted before, most recently by *Krucker et al.* (2005). Although we find this observation intriguing, will not analyze it further in this Chapter.

Topology Observations and Analysis

In order to understand the topological location of magnetic reconnection, we need to characterize the connectivity of the field. An approximation must be made in order to produce the boundaries needed to determine this connectivity. Here, we approximate the field by using a MCT model. Following *Longcope and Klapper* (2002), the line-of-sight

field recorded in magnetograms is partitioned into strong-field regions. Each region is then characterized by a point source which matches the region's net flux and is located at the region's centroid.

In the standard 2.5D model for two-ribbon flares, the CSHKP model (*Carmichael*, 1964; *Sturrock*, 1968; *Hirayama*, 1974; *Kopp and Pneuman*, 1976), the footpoints are predicted to move apart from one another as the reconnection region moves higher in the corona. As field lines are reconnected, the footpoints travel across continuous regions of magnetic flux. In the MCT model, this flux region is represented by a point source, so we cannot follow a footpoint path across it. We can, however, use the concept of spine lines to make the connection between footpoint motion and the MCT model. Spine lines extend across strong-field regions, providing paths through regions of like flux that can be compared to the paths traveled by the HXR footpoints.

As with any coronal field extrapolation model currently available, there are limitations to the MCT model we use. One limitation of our model is the loss of information on the geometry of the field. This is a result of representing patches of magnetic field with point sources. We cannot distinguish if a coronal field line emanates from the outside edge of the modeled source or the center. We are not concerned, however, with the exact location of the topological features of the field – the geometry – but are only interested in the location of topological features relative to each other – the connectivity.

Another limitation of this extrapolation model is that the magnetic field in each domain is potential. Currently, we do not have the ability to model coronal fields above the complex active regions in which flares typically occur with a non-linear force free field model. Nevertheless, a moderately stressed field probably has a topology similar to that of the potential field (*Brown and Priest*, 2000); it has the same separators dividing the flux domains and the same spines modeling photospheric sources.

A third limitation of this MCT model is our inability to consider open field lines or

sheared or twisted flux tubes, whose currents can induce significant topological changes. This means that we cannot fully model the properties of the flux tube which becomes the coronal mass ejection in the CSHKP model. The evidence we have for reconnection deals with electrons streaming along the closed field lines that have collapsed down beneath the separator. Using these closed field lines and the information we have from HXR emission still allows us to point to the topological location of reconnection and thus learn a great deal about the release of energy in flares.

Topological models can be applied more directly to eruptive flares by following flux changes in the strong field regions during the tens of hours prior to a flare. This has been done by *Longcope et al.* (2007) for the 7 November 2004 X2 flare using the Minimum Current Corona model (*Longcope*, 1996, 2001). While using the MCC model certainly has quantitative advantages, it is beyond the scope of this Chapter.

The MCT model produces a topological map at the photosphere which can be used to extrapolate the field into the corona. The calculation of the topology begins by selecting a subregion, namely the main body of the active region, from full-disk MDI magnetograms made as close to the flare start time as is available, typically within 30 min. Next, the observed field is partitioned by grouping pixels that exceed a set threshold (100 G for flares A and B, 50 G for flare C) and are downhill from the local maximum into a region. Regions with fewer than 10 pixels are discarded.

The partitioning determines the location and charge of each pole. A potential field extrapolated from these determines the locations of the nulls. Once the nulls are calculated, the spine lines, separatricies and separators are given by the physics of the MCT model.

The skeleton *footprint*, the intersection of the separatrix surfaces with the photosphere as well as the spine lines, poles and nulls, characterizes the topology of the model and shows the connectivity of the field visually. The area within a domain's boundary, formed in part by the intersection of the separatricies with the photospheric plane and in part by

the spine line, contains the photospheric footprint of the set of field lines connecting the domain's positive and negative poles. The topological footprint for flare A is given in the top panel of Figure 2.4. Source P01, pointed out by the arrow, is connected to many negative sources, including N22, N14, N08 and N13, which are just to the east of P01. For clarity, subsequent figures show only the poles (unlabeled), nulls and spine lines.

We paid careful attention to the co-alignment of the MDI magnetograms and RHESSI data. Spatial alignment of MDI and RHESSI data taken at the same time typically agree to within $2''$ (*Krucker et al.*, 2005). The MDI magnetograms are differentially rotated to the midpoint time of the observed footpoint motion to ensure the best spatial and temporal comparison. One of the criteria for topological analysis of this type is that the flaring region not be more than about 30 degrees from disk center. Outside of 30 degrees, the line-of-sight component of the field is not an accurate enough approximation for our topological models.

Topological analysis gives the connectivity of the field, which is important in this study for two main reasons. One, it aids in the determination of conjugate HXR footpoints. If two HXR sources are conjugate, then there must be field lines connecting the corresponding magnetic sources. Two, the connectivity gives the locations of topological features such as spine lines, which, as we argue in this Chapter, are important analytical tools in the study of reconnection and particle acceleration in flares.

Analysis of Footpoint Motion and Spine Lines

While analyzing the topology of active region 10486 with respect to the HXR footpoints of flare A, we noticed a remarkable visual relationship between the spine lines and footpoint tracks. For example, track 2 (top panel, Figure 2.5) moves through an extended region of negative flux nearly parallel to the spine line. We then expanded our analysis to two different flares, flares B and C, and observed the same relationship. In flare B (center panel, Figure 2.5), the footpoint associated with the positive magnetic field makes two turns, from

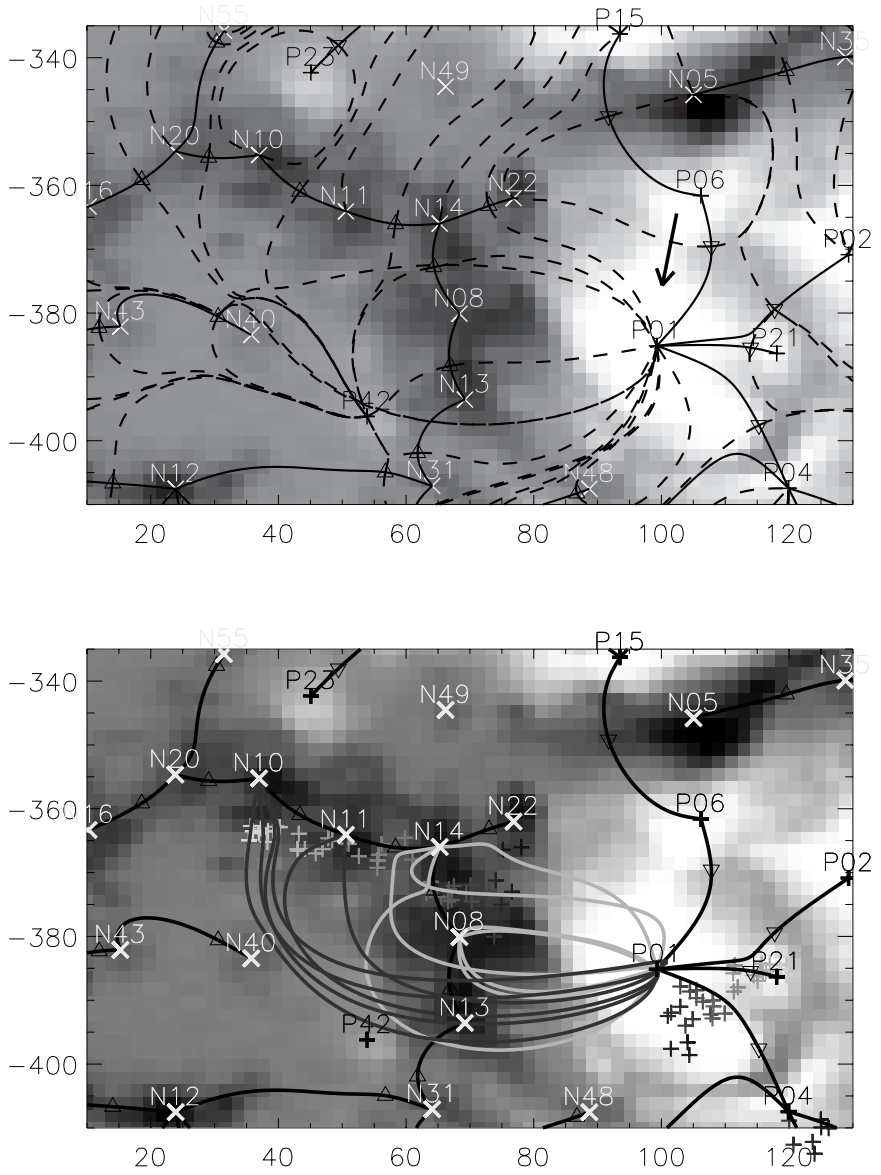

Figure 2.4: Top: photospheric footprint of the topology for flare A. P markers (+) are are positive poles while N markers ($\times$) are negative poles. The triangles are null points, either positive ($\bigtriangledown$) or negative ($\bigtriangleup$). Solid lines are the spine lines and dashed lines are the intersection of the separatrix surfaces with the photosphere plane. The arrow points out pole P01, which is used in an example in the Topology section. Bottom: example field lines for flare A.

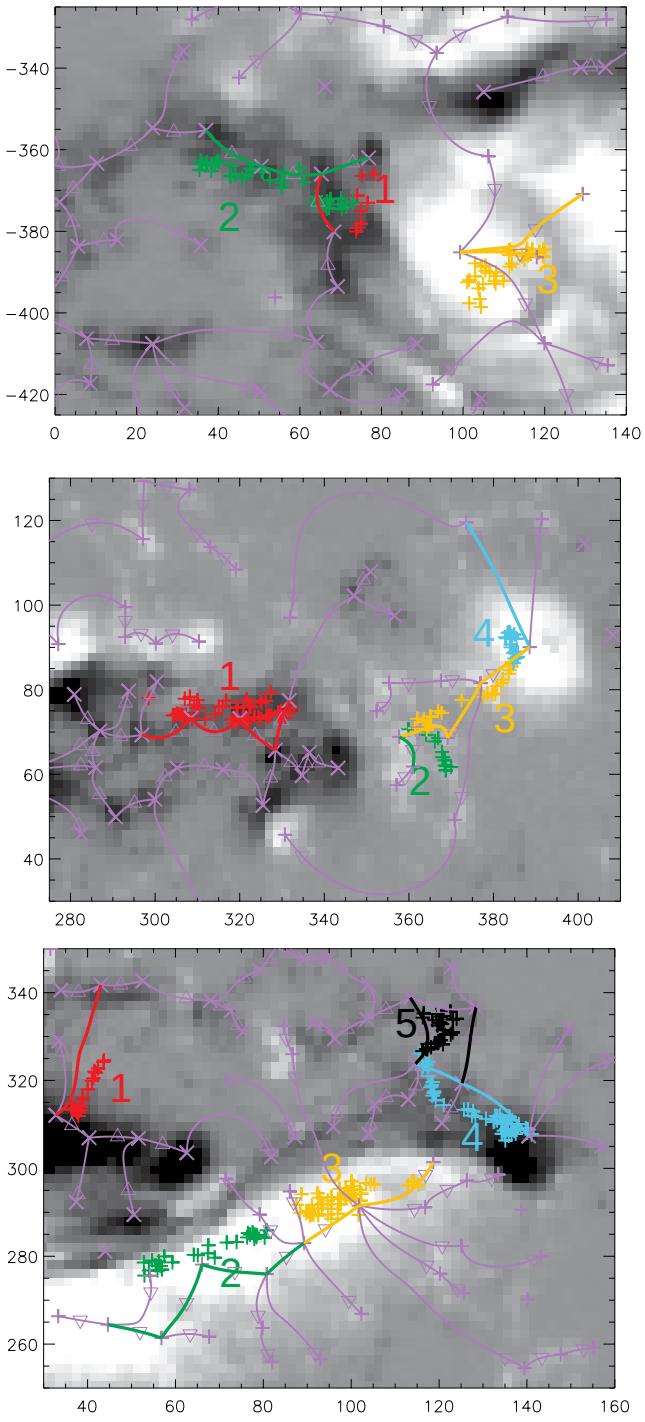

Figure 2.5: Poles, nulls, spine lines and footpoint tracks on magnetograms for flares A (top), B (center) and C (bottom). Violet lines are spine lines which we did not associate with footpoints. Spine lines marked with non-violet colors were identified (and quantitatively analyzed) with the footpoint tracks of like color.

track 2 to 3 and from track 3 to 4, which resemble the spine line curves. As in the first case, the footpoint is moving along an elongated area of flux. The spine lines trace through this flux, connecting a source to an intermediate null to another source. Notice also that this footpoint slows down once it reaches the strong positive region of flux at the end of its path.

Not all footpoint tracks have shapes identical to the corresponding spine line. For example, track 2 of flare C (bottom panel, Figure 2.5) moves in a nearly straight path along the main region of positive flux, while the spine line, due to the locations of the nulls, makes a *W* shape. This discrepancy can be explained by the nature of the topological approximation. As we discussed in the Topology section, information about the geometry of the magnetic field is lost in the process of defining the field's connectivity. The loss of information occurs when boundaries are drawn around source regions and the source regions are represented by point charges. Thus, the location of the spine lines have a spatial uncertainty proportional to the size of the source region. The larger the source region, the larger the uncertainty in the location of spine line. The defining property of a spine line is that it connects regions of like flux. Depending on the characteristics of local maxima in the field, a spine line can take on different paths through the flux regions. We refer again to track 2 of flare C. Here, the spine line reflects the structure of the positive field, but the HXR footpoint simply moves through it.

In order to quantify the association of spine lines and HXR footpoints of the type described above as well as those with a clear visual relationship, we conducted an analysis of the two features' average angles. Due to the nature of the uncertainties in the spine lines, the angle at which the footpoints moved relative to the spines is more important than their distance from the spine lines.

The HXR footpoint angles shown in Table 2.2 were calculated by finding the angle between consecutive centroids and averaging these angles for each footpoint track. Angles

were measured from 0 to 2π radians where 0 rad. always pointed straight to the right of footpoint centroid *i*. If centroid *i* + 1 was located directly north of *i*, then the angle between these footpoints was $\pi/2$. A footpoint moving straight from right to left would have the average angle π. In some cases, footpoints did move steadily in one direction and thus the standard deviation of the angles was small ($\sim$ 0.3 rad). However, in other cases, footpoints moved more randomly and the uncertainty was larger (as large as 1.23 rad.). By integrating over more time when reconstructing RHESSI images, we could have smoothed over some of the small spatial variations. Nevertheless, we wanted to retain a much spatial and temporal information as was allowed by count statistics.

Spine line angles were calculated with the same method as the footpoint tracks, averaging the angles from one point on the spine curve to the next. The uncertainty in the spine angle comes from the fact that a spine can extend from a null at the edge of a flux region across the region in any direction. In our method, the pole is placed at the region's center of flux, such that the spine extends from the null through the center. However, in the un-approximated field the spine line, as an edge of a domain, can extend across the region from the null through any point in the region. Thus, the uncertainty in the spine angle is proportional to the width of the region. To calculate this uncertainty, we measured the angular width of each flux region by finding the angle between two special lines, one drawn from a spine's null to the widest point of the flux region and the other from the spine's null to the center of flux.

Once we calculated the two sources of error – the standard deviation of the footpoint angle and the uncertainty in the spine line angle(s) – we added them in quadrature to produce a total uncertainly. We then checked if each average spine and footpoint angle agreed to within the total uncertainty. Not only was it confirmed that the two angles agreed with each other in every case, but they often matched much more closely than the total uncertainty angle. This can be explained by the fact that our method gives the maximum total

error. If we had simply fit the footpoint track with a line and found how well each HXR centroid agreed with this line, our error would have been smaller. The best fit line method, however, doesn't accurately represent the detailed motion of the footpoints; it smoothes out the short time-scale variations.

Table 2.2 gives the spine line and footpoint track angles as well as their differences. If the spine lines and footpoint tracks were unrelated and their angles were random, then the distribution of their differences would be flat. The distribution is *not* flat, but peaks about 0. Differences in the two angles extends between 0 and $\pi/2$ because spine lines have no temporal 'direction'. We chose to calculate the spine angles in the same direction as the footpoint motion. Thus, the largest the angle differences could have been is $\pi/2$ rad.

In order to quantify the significance of this result, we applied the Kolmogorov-Smirnov (K-S) test (*Press et al.*, 1992) to the unbinned angle differences. The K-S test is the best test for our sample because it assumes nothing about the distribution and uses no bins, both of which can affect the accuracy of other tests. We find that we can reject the null hypothesis that the average spine line and footpoint track angles have a random relationship with 99.95% confidence. Therefore, it is our observational conclusion that the RHESSI HXR sources move along spine lines.

Discussion

In this Chapter, we have demonstrated the association of HXR footpoint tracks and spine lines. Now the question is *why* the HXR footpoints move along spine lines. To understand this relationship, we first need to examine the types of footpoint motion commonly observed. *Somov et al.* (1998) define two categories of flares: more impulsive and less impulsive, acknowledging that some flares are of an intermediate type. They state that in more impulsive flares, which have impulsive phases lasting less than 30-40 s, the HXR footpoints move toward one another. Less impulsive flares, with impulsive phases lasting

Table 2.2: Footpoint track and spine line average angles and their difference.

Flare, Track	Footpoint Angle	Spine Angle	Difference
A, 1	4.13	4.95	0.82
A, 2	3.31	2.96	0.35
A, 3	0.69	0.29	0.40
B, 1	3.34	3.36	0.02
B, 2	2.67	2.00	0.67
B, 3	0.70	0.68	0.02
B, 4	2.20	2.04	0.16
C, 1	1.65	1.23	0.42
C, 2	0.64	0.41	0.23
C, 3	3.51	3.69	0.18
C, 4	2.55	2.55	0.00
C, 5	1.09	1.49	0.40

longer than 30-40 s, undergo an increase in the distance between footpoints. Others (i.e. *Bogachev et al.*, 2005) refer to footpoint motion using descriptions such as motion parallel or perpendicular to the magnetic inversion line.

In the standard 2.5D model for two-ribbon flares, the CSHKP model, the footpoints are predicted to move apart from one another as the reconnection region moves higher in the corona. This separation can only occur *perpendicular* to the magnetic neutral line. The footpoint separation velocity predicted in the standard model is a only few km s^{-1}(*Somov et al.*, 1998). Actual velocities observed by the *Yohkoh* HXT and RHESSI are much larger, on the order of $\sim$ 50 km s^{-1} (see Section 2). Also, the standard model cannot explain footpoint motion with no or decreasing separation, as is often observed (i.e. *Sakao et al.*, 1998). To account for the observed motions and their separation speeds, a 2 or 2.5D model is inadequate; a 3D model is needed. Here, we present such a model, which is an evolution of the 2D CSHKP model into a 3D topological model.

The motion and speed of footpoints along spine lines can be understood with the aid of the quadrupolar model in Figure 2.6. Even in the most complex field, each individual reconnection event involves only 4 domains and therefore can be understood in terms of a

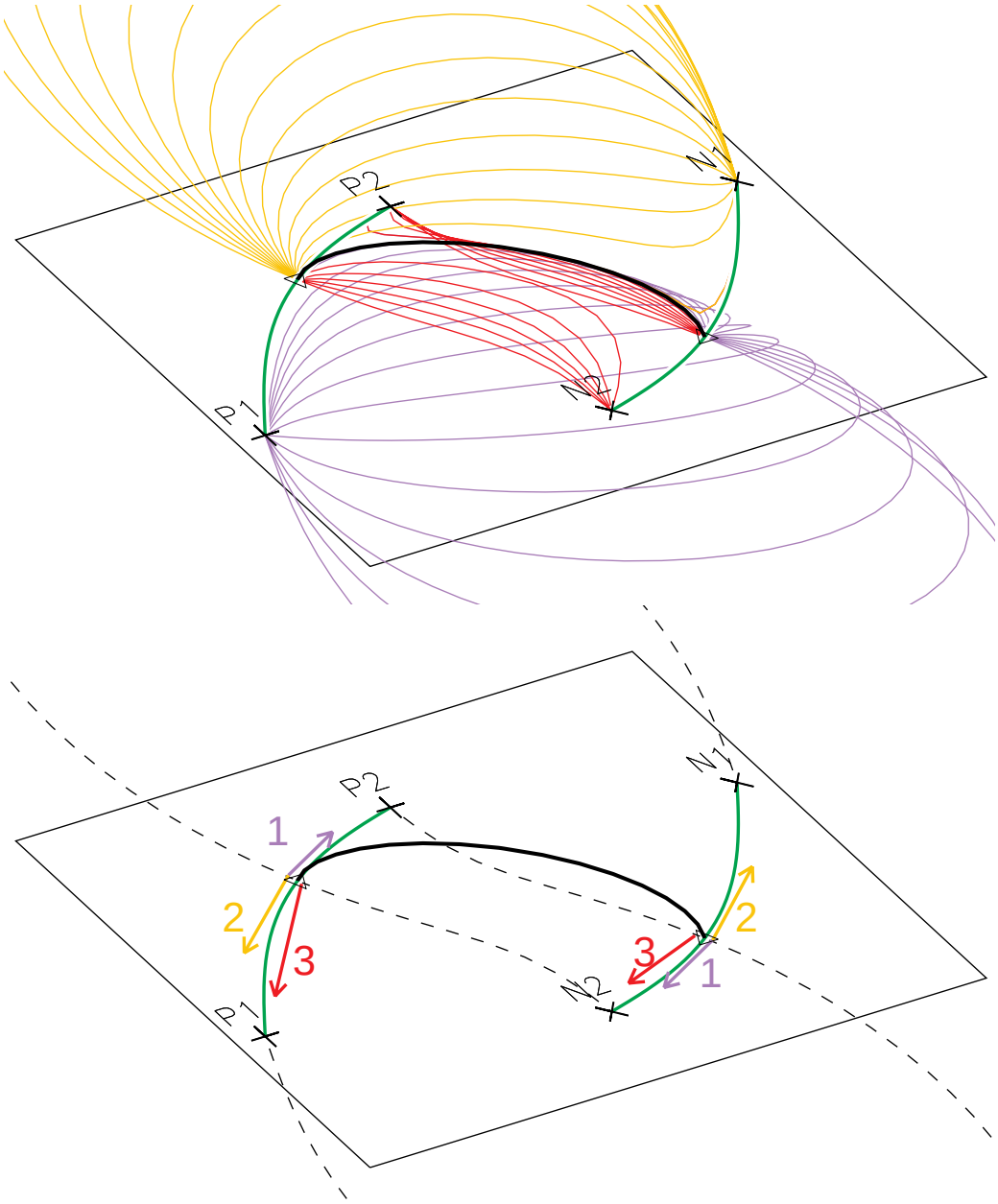

Figure 2.6: Upper panel: key topological features. P2 and P1 (+) are positive poles while N1 and N2 are negative poles ($\times$). The triangles are null points, one positive ($\bigtriangledown$) and one negative ($\bigtriangleup$). The orange, purple and red field lines lie on the separatrix surface under which exist all of the field lines connecting P2/N1, P1/N2 and P2/N2 respectively. Above the orange and purple separatricies is the domain containing all of the field lines that connect P1 to N1. All four of these domains intersect at the separator (thick black line). The thick green lines are the spine lines. Lower panel: expected footpoint movement along the spine lines for the configuration in the upper panel. Dashed lines are the intersections of the separatrix surfaces with the photosphere. Arrows indicate the direction of separator movement during reconnection for cases 1, 2 and 3 (see the Discussion section).

quadrupolar configuration. The quadrupolar configuration is not meant to model the entire flaring region, but rather, the separator in the configuration is one of several on which reconnection occurs over the course of a flare.

We discuss three cases of reconnection events for this quadrupolar model. In each case, reconnection is the result of a flux imbalance in part of the quadrupolar configuration. As a flare progresses, the reconnection moves from separator to separator (thus from one quadrupolar region to another), balancing the flux and reducing the energy state of the magnetic field. More complete details on the way we understand how reconnection transfers from one separator to another are given in a paper recently submitted by *Longcope and Beveridge* (2007).

The assumptions involved in our explanation include the following. Reconnection occurs at a current sheet which is located on the separator, producing fast-precipitating electrons which stream along the separator field line until they encounter the chromosphere. At the chromosphere, the electrons are decelerated via thick-target bremsstrahlung, resulting in the HXR footpoint sources.

We point out that linked spine lines are the topological characterization of extended regions of like flux. The MCT extrapolation model's point sources (poles) represent patches of photospheric flux. The poles are placed at patch's center of flux. Between two poles exists a place where the field strength goes to zero (a null). A single spine line connects two like poles via the null. Often, a spine line links not just one pair of poles, but continues to another null and then another pole, and so on. It is not surprising, therefore, that the HXR footpoints move along the spine lines, especially in the cases where the magnetic flux is strung out in fragmented pieces as in track 2 of flare A. The correlation, however, between spine lines and non-fragmented flux is also significant. For example, track 3 of flare C, which extends through a solid area of flux, corresponds to the spine line to within 0.18 rad.

In case 1, we suppose that the domain P2/N2 (containing the red field lines) has too much flux in the sense that it can reach a lower energy state (become more potential) by decreasing its flux through reconnection. Also, let's say the separator in the figure is at the position drawn at time t=0. If a field line from the underlying flux domain P2/N2 approaches a field line in the overlying domain P1/N1 at the separator and reconnects, producing two new field lines in the domains P2/N1 (orange) and P1/N2 (purple), then the reconnected flux is moved from P2 into P1 and from N2 into N1. At a later time t=1, the separator is located closer to the P2 source center due to P2's loss of connecting field lines and P1's gain. The other end of the separator is closer to N2's center due to N2's loss and N1's gain. As time goes on, the process of P2 losing field lines to P1 and N2 to N1 continues, and the chromospheric ends of the separator (and hence the HXR footpoints) move antiparallel and slightly *toward* each other along the spine lines, shown by arrows in Figure 2.6.

Somov et al. (1998) present a different analysis reaching a similar conclusion. In their topological model 'more impulsive' flares have decreasing longitudinal magnetic flux along the separator, resulting in a decrease in the distance between footpoints. They also point out that the reconnected field lines decrease in length as the reconnection process proceeds. This is the same basic physical process we describe in case 1, with the exception that we refer specifically to how the *separator* changes rather than the decrease of longitudinal flux and reconnected field line length. In case 1, the separator would shorten in length and decrease in height as the domain beneath it shrank.

In case 2, we suppose that the domain P2/N2 (red) has too little flux, so field lines from the domains P1/N2 (orange) and P2/N1 (purple) reconnect to form new lines in P1/N1 and P2/N2. Here, the footpoints move towards the N1 and P1 centers of flux, antiparallel and *away* from each other along the spine line. The separator lengthens and increases in height as the domain beneath it grows.

This example is similar to the reasoning used to explain two ribbon flares with sheared arcades. When a sheared magnetic field suddenly releases energy in the form of a two ribbon flare, domains of source pairs initially far apart and nearly empty of flux now have too little flux relative to a lower-energy field. In order to lower the energy state, flux is added to the underlying deficient domains, reducing the shear in the field and increasing the length and height of the separator. The separator current sheet moves along the spine lines, sweeping through equal areas of positive and negative photospheric flux and the flare footpoints move apart. The magnetic sources themselves don't change–only their connectivity does so.

In case 1 the imbalance of flux led to the growth of both center domains P1/N2 and P2/N1 (purple and orange) and case 2 led to their shrinkage. In case 3, we deal with the final possibility of flux transfer in a quadrupolar configuration – when there is a flux imbalance in one of the center domains with respect to the other. For example, we assume the domain P1/N2 has too much flux and it can reach a lower energy state by transferring flux from domains P1/N2 (purple) and P1/N1 (overlying) into domains P2/N1 (orange) and P2/N2 (red). In this process, the entire separator shifts along the magnetic neutral line as the footpoints move *parallel* to each other towards the P1 and N2 poles. Parallel HXR footpoint motions are often observed; for example, *Bogachev et al.* (2005) report that 35% of the flares they observed had HXR footpoint sources that moved in the same direction.

To summarize, footpoint motion along spine lines corresponds to movement of the reconnection location. As the separator current sheet sweeps across region of flux, its chromospheric ends either move toward each other (compact flare; case 1) as the separator shortens, the ends move away from each other (eruptive two ribbon flare; case 2) as the separator lengthens or the ends move parallel to each other (case 3) as the separator stays approximately the same length. The movement of the separator's chromospheric ends, and hence the HXR footpoints, is along the spine lines. Spine lines connect two poles via a

null which shifts during the flare toward one pole or the other. The direction the null shifts depends on the global configuration of the region; the underlying domain gains or loses flux in order to decrease the region's energy state.

The above explanation agrees with the observed footpoint tracks and footpoint separation speeds of the three flares reviewed in this Chapter. Referring again to Figure 2.4, we propose the following explanation for the footpoint motions of flare A. As is indicated by the number of light grey field lines drawn in domains P01/N14 and P01/N08, a large percentage of P01's flux is connected to N14 and N08. Initially, the footpoint separation distance decreases due to the reconnection of flux out of underlying domains P01/N14 and P01/N08. The next stage of reconnection acts to release energy stored in the sheared arcade. Domains which have little connecting flux in the earlier stage of the flare (P01/N11 and P01/N10) fill up as reconnection takes place on higher and longer separators, and the footpoints move apart from one another. An in-depth analysis of separator properties before and after flares will be given in a subsequent paper.

Our model can be compared to other models that have been proposed to explain HXR footpoint source motions. *Bogachev et al.* (2005) use a sheared 2.5D model to explain the antiparallel motion of HXR footpoints along the neutral line. In their model, which cannot distinguish between flares with increasing footpoint separation from flares with decreasing separation, the apparent motions of HXR sources are determined by the order of reconnection along the sheared system of field lines. During the onset of a flare, the footpoint sources move toward each other, decreasing the distance between them, until a critical point is reached and the sources begin to move away from one another. This model is similar to other models of reconnection in sheared arcades, where reconnection starts on the most highly sheared field lines and progresses to the less sheared field higher in the corona. As was pointed out earlier in this section, case 2 of our model is analogous to these models where reconnection in sheared fields leads to the antiparallel motion of HXR footpoint

sources. In this case, the flux deficiency in the underlying domains, due to the shear in the initial configuration, leads to reconnection that increases the length of the separator, and consequently, the footpoint separation increases.

Our model is also comparable to the slip-running reconnection model proposed by *Aulanier et al.* (2006), which describes reconnection within the framework of QSLs. In complex 3D magnetic configurations, QSLs become separatrices as their width approaches zero. In fact, the intersection of QSLs with the chromosphere are similar to spine lines in that they extend from one magnetic flux source to another of the same polarity. Within the QSL, the sub-region where the squashing degree Q (*Titov et al.*, 2002) peaks (where the connectivity gradients are the largest) is known as the hyperbolic flux tube (HFT: *Titov et al.*, 2003). A HFT becomes a separator as its squashing degree asymptotically tends to infinity. *Aulanier et al.* (2006) state that QSL reconnection leads to field line slippage along the QSLs and thus the field lines slip-run along the intersection of the QSLs with the line-tied boundary. In this reconnection process, particles are accelerated to their highest energies in the HFT, so HXR emission is expected at the chromospheric ends of the HFT. Given this and the fact that the intersection of the QSLs with the chromosphere correspond to flare ribbons (i.e. *Démoulin,* 2006), slip-running reconnection is a possible explanation for the motion of HXR sources along flare ribbons. Due to the analogies between the intersection of QSLs with the chromosphere and spine lines, as well as between HFTs and separators, we suggest that slip-running reconnection is the QSL version of the separator reconnection modeled in this paper. Our separator reconnection model, however, is significantly less time consuming than the QSL method; only a few QSLs have been calculated for flaring active region magnetic field configurations.

The association of footpoints tracks with spine lines, and more importantly the physical explanation for the association, can be used in future flare analysis. Having an explanation for why HXR footpoints move the way they do will aid in the understanding of flare ini-

tiation and evolution. Further work with topological models, especially analysis involving the role of separator current sheets, is needed to understand this and other aspects of the flaring process.

CHAPTER 3

A NEW TECHNIQUE FOR REPRESENTING PHOTOSPHERIC MAGNETIC FIELDS IN TOPOLOGY CALCULATIONS

Abstract

In this Chapter, I describe a new method for representing active region magnetic fields in magnetic charge topology (MCT) models. The topology calculation of an active region is determined by a representation of the photospheric magnetic flux sources. Typical MCT photospheric representations characterize a sub-region's magnetic field by a single point source located at the sub-region's flux centroid. While this method is quantitative, it cannot describe internal changes and rotations of sub-regions, which are thought to store energy prior to a flare. Here, I illustrate a new method that can portray these types of sub-region changes by representing the sub-regions with three point sources rather than one. I compare the topological features produced by the new method to those produced by the original method in two cases: a simple simulated magnetic configuration and a flaring active region. I find that the detail given by the new method enables a level of topological analysis not possible with the original method.

Introduction

Magnetic reconnection is the mechanism of topological change that is thought to bring about energy release and non-thermal electron acceleration in solar flares. By studying the radiative output of flares in association with the magnetic topology of the flaring region, we can learn a great deal about the topological location of reconnection. For a study of this type to be successful, the topology calculation needs to quantitatively characterize the

photospheric and coronal magnetic field and have quantitatively defined features.

One commonly used topological model that fulfills these requirements is a type of magnetic charge topology model (MCT; see *Longcope*, 2005) where each region of strong photospheric flux is replaced by a single point source at the solar surface. While this MCT method is quantitative, its representation of the observed photospheric field lacks the detail necessary to analyze internal changes and rotations of magnetic flux sources. These changes are theorized to be of key importance in the build up of energy prior to a flare (*Beveridge and Longcope*, 2006). In this Chapter, I describe a new, more detailed photospheric representation and compare the topological features produced by it to those produced by the original representation.

MCT models assume that the photospheric field of an active region can be partitioned into distinct unipolar sub-regions. Also, they assume that any two field lines with both their footpoints in the same sub-region are topologically equivalent (*Longcope*, 2005). As a result of the first assumption, coronal field lines are anchored in discrete flux sub-regions separated by a contiguous region in which the normal component of the magnetic field is zero.

In the type of MCT model used here, these sub-regions of flux, which are observed in Solar and Heliospheric Observatory/Michelson Doppler Imager (SOHO/MDI; *Scherrer et al.*, 1995) line-of-sight magnetograms, are replaced by a multipole expansion. The original point source MCT method approximates a sub-region with a single point source, or *pole,* located at the region's center of flux. This matches the true field out to the second term (dipole) in the multipole expansion.

While the dipolar expansion of sub-region flux sources is a sufficient representation of the photospheric field for some studies, others require a more detailed one. For example, if I wish to examine how internal changes and rotations of sunspots affect the coronal field, I need a model that characterizes the sub-regions with more than one pole. A multipole

expansion that matches the true field of the sub-region out to the third term (*quadrupole)* would improve the accuracy of the coronal extrapolation and enable a more in-depth analysis of photospheric magnetic field changes. A single pole cannot give a multipole expansion because its quadrupole moments are zero. Therefore, I developed a new method for characterizing the photospheric field of an active region where sub-regions are represented by a quadrupolar expansion by replacing each sub-region with three sources.

In the Method section, I describe the method I use to define quadrupolar expansions of the sub-region flux sources. In the Analysis section, I use a simulated magnetogram and a real magnetogram to analyze the differences between the original dipolar method and this new quadrupolar one. Finally, I discuss the results of my analysis and give my conclusions in the Discussion and Conclusions section.

Method

The technique I use to improve the MCT extrapolation model is to replace the original dipolar expansion of each magnetic field sub-region that exceeds the set amount of flux with a quadrupolar expansion. In the original version, the magnetic flux of a sub-region is represented by one point source with equivalent flux located at the sub-region's center of flux, ($\overline{x}, \overline{y}$),

$$\overline{x} = \frac{1}{\Phi} \int \int x \cdot B_z(x, y) dx dy, \tag{3.1}$$

$$\overline{y} = \frac{1}{\Phi} \int \int y \cdot B_z(x, y) dx dy, \tag{3.2}$$

where

$$\Phi = \int \int B_z(x, y) dx dy. \tag{3.3}$$

Here, $B_z(x,y)$ is the value of the vertical field (approximated by the observed line-of-sight field) for each (x,y) position and Φ is the sub-region flux. In order to extend the multipole expansion to the next (quadrupole) term, more than one source must be used because the quadrupolar moments of a single point source are equal to zero. The three terms, $Q_{r,xx}$, $Q_{r,xy}$, and $Q_{r,yy}$, of the quadrupolar moment tensor for the real magnetic sub-regions are given by

$$Q_{r,xx} = \int\int B_z(x,y)(x-\overline{x})^2 dxdy, \tag{3.4}$$

$$Q_{r,xy} = \int\int B_z(x,y)(x-\overline{x})(y-\overline{y}) dxdy, \tag{3.5}$$

$$Q_{r,yy} = \int\int B_z(x,y)(y-\overline{y})^2 dxdy. \tag{3.6}$$

To match the quadrupolar moments (three constraints), flux (one constraint) and centroid position (two constraints), of the real magnetic sub-region to the quadrupolar moments, $Q_{m,xx}$, $Q_{m,xy}$, $Q_{m,yy}$, flux, and centroid position of the model sources, six degrees of freedom are needed. Using two poles rather than one will give the required degrees of freedom, two for the source magnitudes and four for the source locations. With only two sources, however, $Q_{m,xx}Q_{m,yy} = Q^2_{m,xy}$, which means that not all quadrupolar tensors can be represented. Therefore, three sources are needed to represent each sub-region of magnetic flux.

The quadrupolar moments of the three sources, which are matched to the quadrupolar moments of the real sub-region are

$$Q_{m,xx} = \frac{1}{3}\Phi(x_1^2 + x_2^2 + x_3^2), \tag{3.7}$$

$$Q_{m,xy} = \frac{1}{3}\Phi(x_1 y_1 + x_2 y_2 + x_3 y_3), \tag{3.8}$$

$$Q_{m,yy} = \frac{1}{3}\Phi(y_1^2 + y_2^2 + y_3^2). \tag{3.9}$$

Here, in order to simplify the required calculations, I have removed two of the nine degrees of freedom by assuming each of the three point charge fluxes is equal to 1/3 of the sub-region's flux. For added convenience, I move the calculation to a frame of reference located at the center of flux, ($\overline{x}$, $\overline{y}$), so that I can set $x_3 = -x_1 - x_2$ and likewise for y. I use the remaining seventh degree of freedom to minimize L, the perimeter of the triad,

$$L = |\boldsymbol{X_1} - \boldsymbol{X_2}|^2 + |-\boldsymbol{X_1} - 2\boldsymbol{X_2}|^2 + |-2\boldsymbol{X_1} - \boldsymbol{X_2}|^2 \tag{3.10}$$

which makes the three pole representation more compact. Here, $\boldsymbol{X}$is the (x,y) vector in the center of charge reference frame (i.e. $x_3 = -x_1 - x_2$). The problem thus has four equations (three for the quadrupolar moment and one minimization) and four unknowns (two x,y positions).

I solve for the locations of the point charges by using Singular Value Decomposition (SVD). I have three equations with four unknowns, so I use the *Newton-Raphson* method to get a set of solutions, then do the minimization to find the solution with the smallest perimeter. Once the equations are solved for the source positions representing each sub-region, I convert the positions back to the initial, non-center-of-flux reference frame. The result of these calculations is a compact configuration of point sources that defines a multipole expansion of the observed flux sub-region out to the quadrapole term.

Once the multipole expansions of the magnetic sub-regions within an active region have

been determined, several other topological features can be defined. Each coronal field line is assigned to a flux *domain* according to the poles at each of its two footpoints. *Nulls* are the locations between like signed poles where the magnetic field strength is zero. A special field line, the *spine* line, extends from a pole through a null to another pole of the same polarity. The two poles connected by the spine line via the null are the null's *spine poles*. The surfaces dividing domains are *separatrix* surfaces, which are the *fan* surfaces of the null points. Two separatrix surfaces intersect along a *separator*, the three dimensional analog to a two dimensional X point. A separator is the location reconnection must occur in the three dimensional MCT coronal model.

Two features of importance to my study of the topological location of reconnection are nulls and separators. The nulls given by this more detailed method can be categorized into level 1 and level 2 nulls. Level 1 nulls are typically the same as the nulls in the dipolar expansion method; they are located between different sub-regions of like sign. Their spine sources belong to different regions, so their fan surface (separatrix) divides flux enclosed in different sources. Level 2 nulls are those that exist between sources within a single sub-region. Here, the spine sources belong to a common region, so their fan surface creates an 'internal' division.

Separators can be categorized based on the type of nulls at their photospheric ends. Those with both ends at level 1 (2) nulls are level 1-1 (2-2) separators. Those with one end at a level 1 null and the other at a level 2 null are level 1-2 separators. It is theorized that level 1-1 separators are analogous to the separators defined by the dipolar method because their nulls are similar. Level 1-2 and 2-2 separators connect to nulls within flux sub-regions and can thus give information about the rotations and internal changes of sub-regions.

Analysis

In order to analyze this quadrupolar representation of photospheric magnetic flux sources

with reference to the previously used dipolar expansion, I examine the topological features produced by both methods in the cases of a simple simulated magnetogram and a real MDI magnetogram. To illustrate the differences between the two methods in simple case, I created a fake magnetogram by placing four ellipses, two positive and two negative, of different sizes and shapes in a region of otherwise blank 'field'.

In the simulated example, shown in Figure 3.1, the two nulls given by the dipolar method are located between the two regions of like flux. In the quadrupolar expansion, shown in Figure 3.2, the two level 1 quadrupolar nulls are located in similar locations to the two dipolar nulls. The quadrupolar method, however, has two additional level 2 nulls present between sources within each sub-region. While there is only one dipolar separator, there are 12 quadrupolar separators: one level 1-1, six level 1-2s and five level 2-2s. Both the dipolar and quadrupolar topological features are shown in Figure 3.3 for direct comparison. This example makes it clear that the quadrupolar method is a more detailed representation of the magnetic field.

As an example of a flaring active region, I examine the dipolar and quadrupolar topological features resulting from an MDI magnetogram recorded at 12:51 UT 6 April, 2004. In Figures 3.4 and 3.5, I plot the dipolar and quadrupolar topological features, respectively. So that they can be compared directly, I also show both sets of features in Figure 3.6, where the dipolar features have been plotted after the quadrupolar features. The topology calculations for this active region produced 17 separators in the dipolar expansion and 51 separators in the new quadrupolar version.

At 13:22 UT, this active region produced a M class flare with two hard X-ray (HXR) footpoint sources, one in the main region of positive polarity (center of Figure 3.6) and one in the negative polarity region to the northeast. There are no dipolar separators connecting the two sub-regions where the HXR sources appeared, but there are several level 1-2 and 2-2 quadrupolar ones. This suggests that the flare was powered by reconnection between

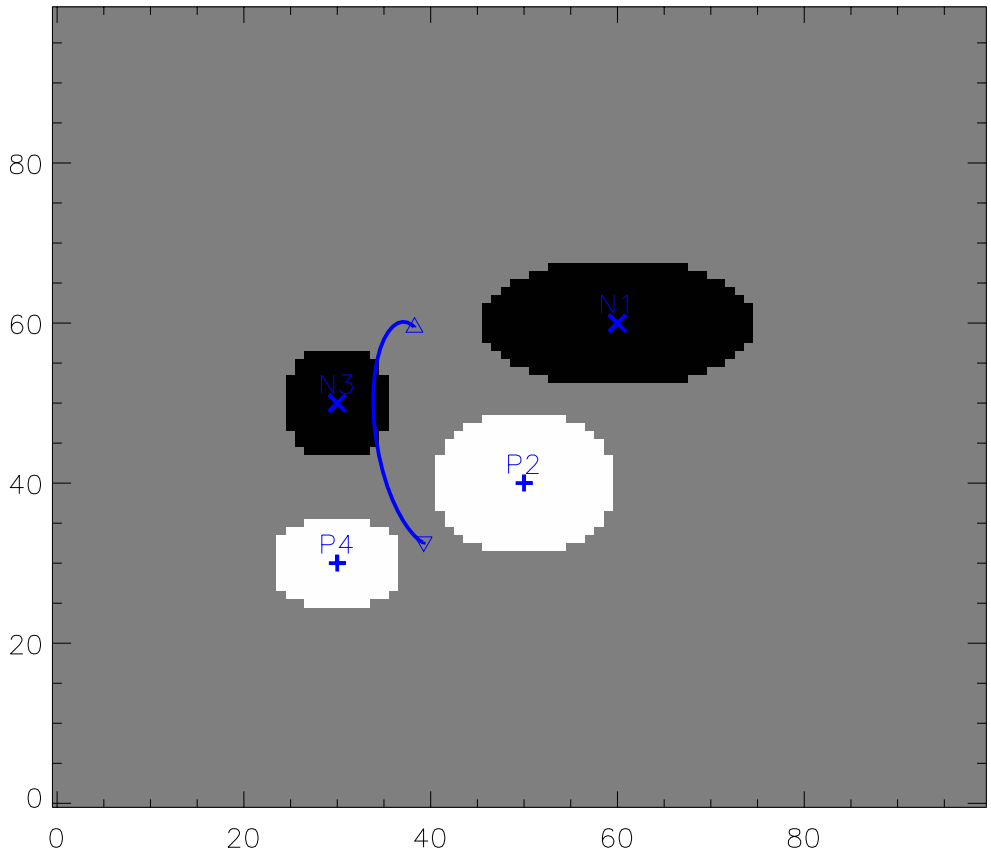

Figure 3.1: Simulated magnetogram with dipolar features. dipolar poles (+ positive, $\times$ negative) are labeled by a capitol letter and a number. Nulls are indicated by triangles ($\bigtriangledown$ positive, $\bigtriangleup$ negative), and lines are separators.

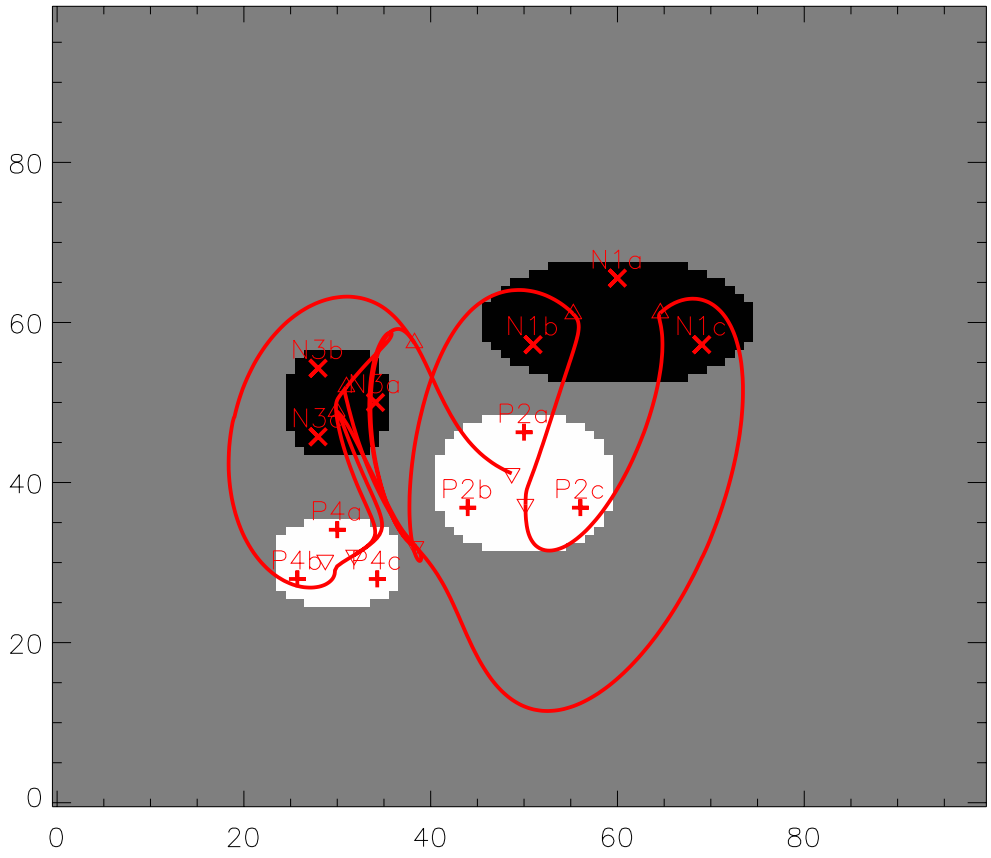

Figure 3.2: Same as Figure 3.1, but with quadrupolar features. Quadrupolar poles have an additional lower-case letter as a third character in their label.

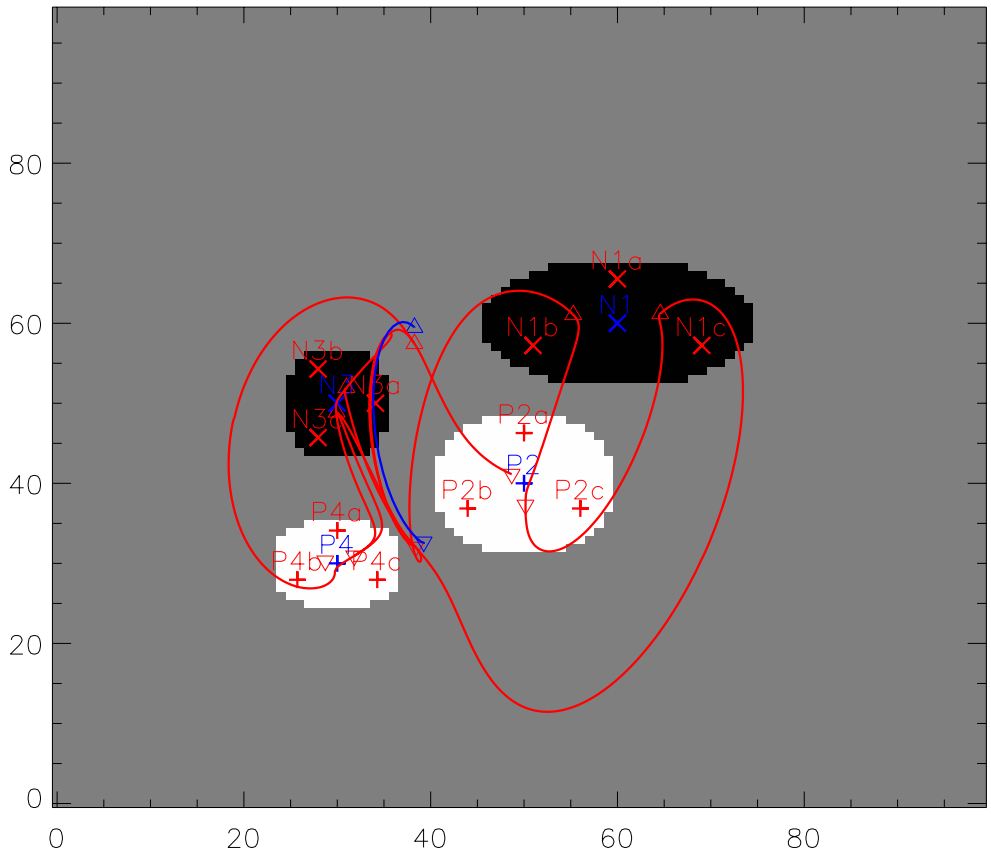

Figure 3.3: Same as Figure 3.1, but with both dipolar (blue) and quadrupolar (red) features for comparison.

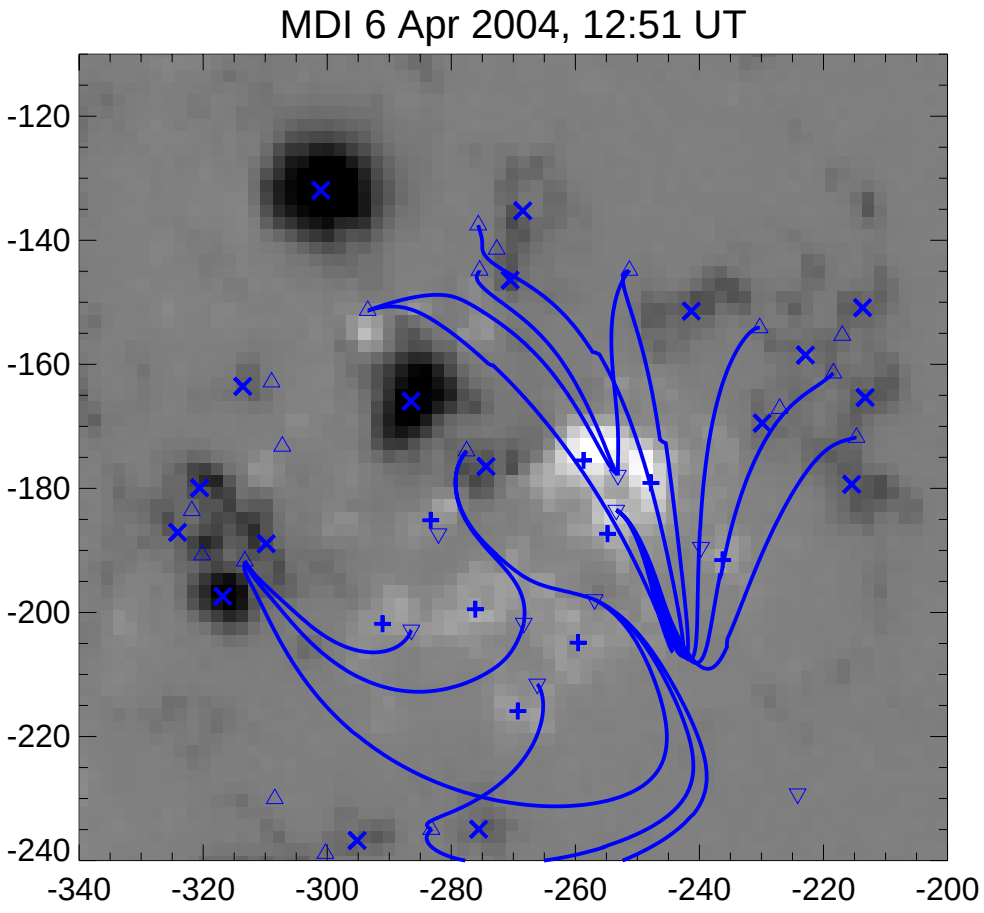

Figure 3.4: MDI magnetogram with dipolar poles, nulls and separators.

domains internal to the source regions. Therefore, the topological location of magnetic reconnection could not be examined in this case without the quadrupolar expansion method (see Chapter 4).

Discussion and Conclusions

My analysis of the topological location of magnetic reconnection proceeds under the following working hypothesis. In the absence of major reconnection, coronal magnetic fields become stressed as the photospheric boundary slowly evolves due to the emergence

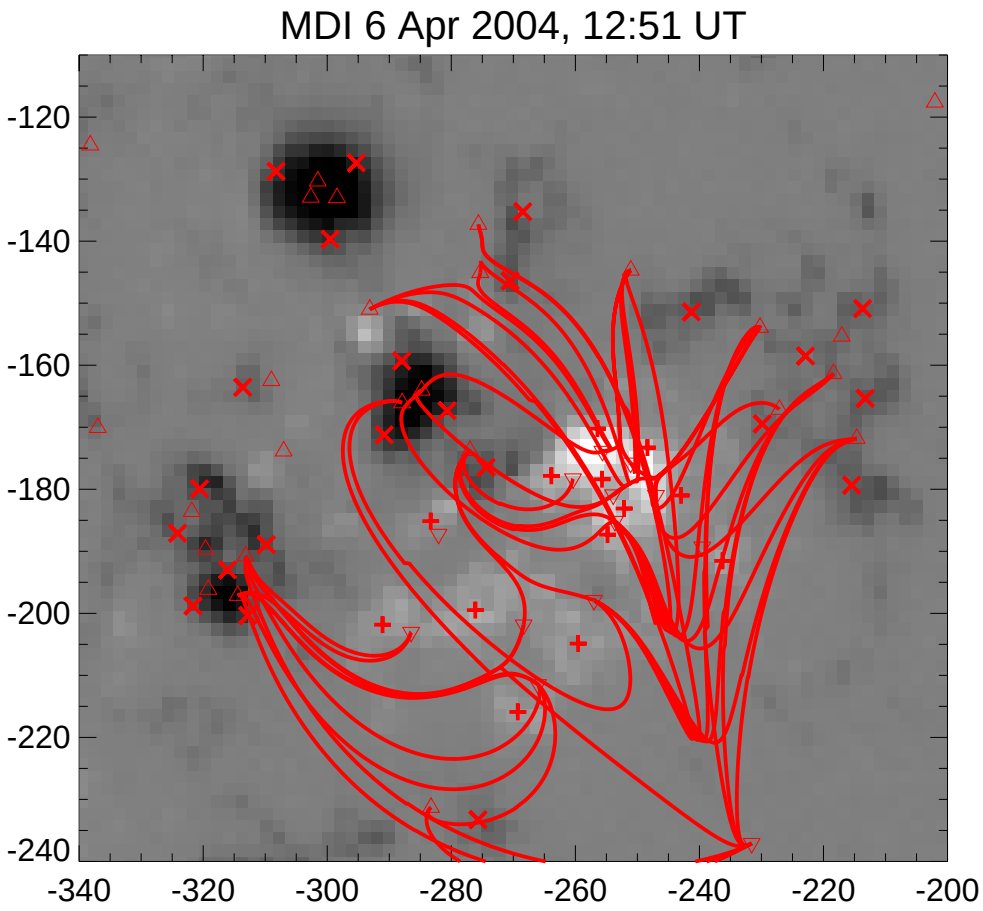

Figure 3.5: Same as Figure 3.4, but with quadrupolar features.

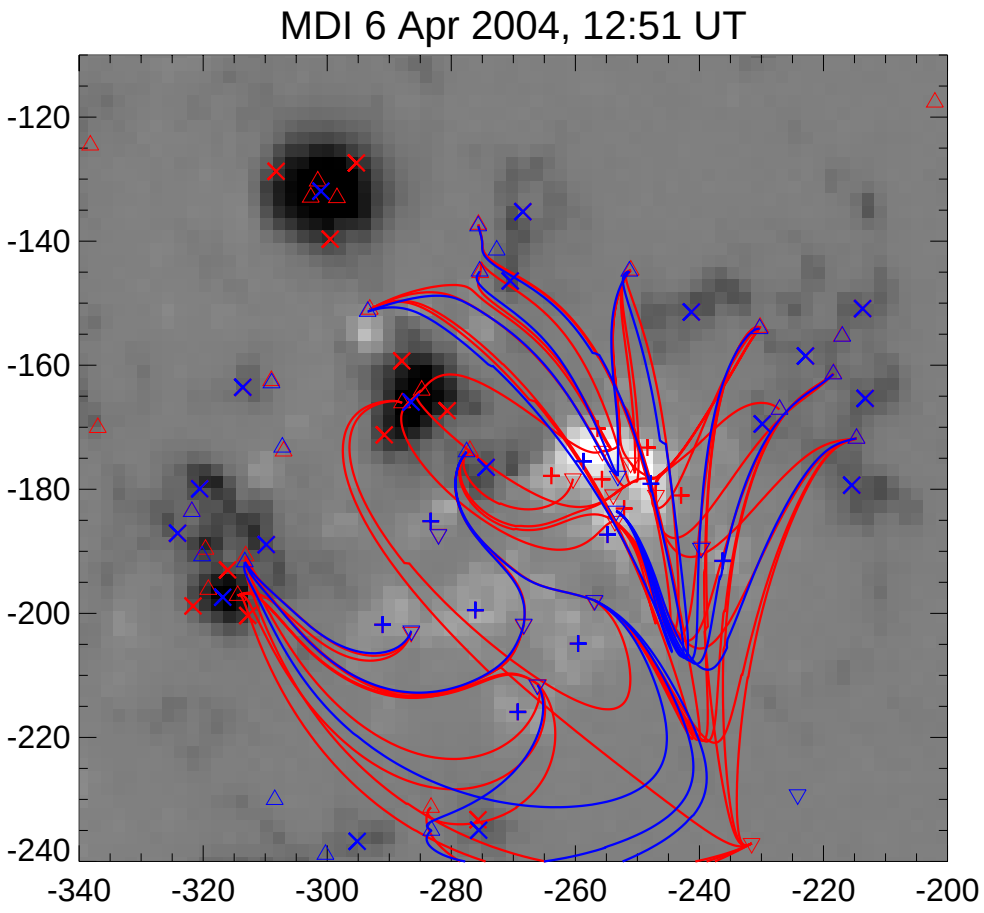

Figure 3.6: Same as Figure 3.4, but with both dipolar (blue) and quadrupolar (red) features.

of new field and horizontal flows. When a critical point is reached, this energy is released by the rapid reconnection of magnetic field lines near the separator. As a result, electrons are accelerated near the reconnection region and stream along field lines near the separator. Upon encountering the chromosphere, the electrons undergo bremsstrahlung and non-thermal HXR are emitted. Thus, HXR footpoint sources can be interpreted as the location of the chromospheric ends of newly reconnected field lines, which lie close to the separator.

Based on this working hypothesis, separators are the link between the reconnection region and HXR footpoint sources. In order to examine the topological location of reconnection, I need a topological model that is detailed enough to produce separators that connect to nulls within strong magnetic flux regions. While the original MCT model is quantitative, it does not, by definition, produce the required separators. The original MCT dipolar expansion represents each magnetic sub-region with a single point source, so all of the nulls present in the photospheric representation are located *between* the sub-regions. The new version of the MCT model described in this Chapter increases the detail in the photospheric representation by characterizing the sub-regions with a quadrupolar expansion. This quadrupolar expansion produces nulls and separators between sources within a single sub-region. Therefore, it can be used to study internal changes and rotations of sub-regions and thus enables the examination of the topological location of magnetic reconnection. This examination and its results are described in Chapter 4.

CHAPTER 4

SIGNATURES OF MAGNETIC STRESS PRIOR TO THREE SOLAR FLARES OBSERVED BY RHESSI

Abstract

We examine the hard X-ray (HXR) footpoint sources of three flares, as observed by RHESSI, in combination with the topology given by the extrapolation of line-of-sight magnetograms into the corona. Assuming the HXR footpoint sources are chromospheric consequences of magnetic reconnection that takes place on separators, we further assume a relationship between the build-up of energy in stressed coronal magnetic fields and the measurement of the change in separator flux per unit length. We find that the value of this quantity is larger on the separators that connect the HXR footpoint sources than the quantity on the separators that do not. Therefore, we conclude that we are able to understand the location of HXR sources observed in flares in terms of a physical and mathematical model of the topology of the active region.

Introduction

By combining flare hard X-ray (HXR) observations with three dimensional topological models of active region coronal magnetic fields, we can expand the available tools for understanding where solar flares occur within active regions. HXRs are a signature of the presence of high-energy electrons, which are believed to originate in magnetic reconnection. Magnetic reconnection is commonly accepted as the key physical process in the release of energy stored in stressed coronal fields. The energy available to power flares is thought to be stored in the magnetic field in the form of currents positioned near sep-

arators (*Henoux and Somov*, 1987). Separators are the three dimensional analogs of two dimensional X-points; they are the location of reconnection in three dimensional models (*Gorbachev and Somov*, 1988). This motivates the testable hypothesis that HXR emission is associated with the separators at which reconnection has taken place.

Our analysis of the topological location of magnetic reconnection proceeds under the following working hypothesis. In the absence of major reconnection, coronal magnetic fields become stressed as the photospheric boundary slowly evolves due to the emergence of new field and horizontal flows. When a critical point is reached, this energy is released by the rapid reconnection of magnetic field lines near the separator. As a result, electrons are accelerated near the reconnection region and stream along field lines near the separator. Upon encountering the chromosphere, the electrons undergo bremsstrahlung and non-thermal HXR are emitted. Thus, HXR footpoint sources can be interpreted as the location of the chromospheric ends of newly reconnected field lines, which lie close to the separator.

Past research on energy storage prior to a flare has concentrated on non-potential signatures in vector magnetograms (i.e. *Gary et al.*, 1987; *Wang et al.*, 1996; *Moon et al.*, 2000; *Deng et al.*, 2001; *Tian et al.*, 2002; *Falconer et al.*, 2006; *Dun et al.*, 2007). For example, *Dun et al.* (2007) calculated the daily average values of three non-potential parameters from vector magnetograms: magnetic shear angle, line-of-sight current, and current helicity of selected regions along the main neutral lines of active region 10486. They found that the three non-potentiality parameters increased at the impulsively brightening flare sites from values measured at least one day before the two large X-class flares of 28 and 29 October, 2003. *Dun et al.* (2007) also study the magnetic flux evolution in the brightening regions and find an increase in magnetic flux and complex proper motions concurrent and co-spatial with the increases in non-potentiality.

Another way to examine the build up of energy prior to a flare is by using the Minimum

Current Corona model (MCC; *Longcope*, 1996, 2001). The MCC model tracks the complex evolution of photospheric flux to determine the lower bound on the energy stored by this motion. *Longcope et al.* (2007) calculate the MCC model for the 7 November 2004 X2 flare and find that the predicted flux reconnected during the flare compares favorably with values inferred from motions of the flare ribbons and the magnetic cloud. It is not necessary, however, to do the full MCC calculation to find where within an active region energy is preferentialy stored, which is the goal of this Chapter. We employ a restricted form of the MCC whereby we use separators to estimate the locations of energy accumulation. We hypothesize that these two methods, the MCC model and the calculation done here, examine the same fundamental physics – the relationship between the motion of photospheric sources and the build-up of energy in the line-tied coronal field.

In order to make the connection between the energy released in solar flares and the location of energy storage in the non-potential components of the magnetic field, a magnetic field model is needed. The standard flare model, CSHKP (*Carmichael*, 1964; *Sturrock*, 1968; *Hirayama*, 1974; *Kopp and Pneuman*, 1976), describes a two dimensional morphology where energy is stored in a stressed coronal field. Rapid reconnection takes place at the X point, which divides the open field line domian from the closed one, reconfiguring the coronal field and converting magnetic energy into particle acceleration, heating and kinetic energy. Since some of the electrons accelerated in the reconnection process stream along the newly formed field lines and bombard the relatively dense chromosphere in a fraction of a second, the location and timing of flare emission observed in Hα, UV and HXR is a useful link to coronal reconnection location and timing.

One way the CSHKP model can be linked to energy release is by relating the properties of two-ribbon flares observed in Hα and UV to the rate of reconnection in the corona. Here, flare ribbons are taken to be the photospheric/chromospheric intersection of the separatricies dividing the open field line domain from the closed field line domain. Due to

the line-tied nature of the photospheric magnetic field, motion of the ribbon is a signature of the moving separatrix (*Forbes and Lin*, 2000). Assuming a two dimensional field, Faraday's equation can be used to relate the uniform electric field along the reconnecting current sheet to the rate at which magnetic flux is reconnected, $E = B_n V_r$, where B_n is the normal component of the magnetic field and V_r is the apparent motion of the ribbon perpendicular to the neutral line (*Forbes and Priest*, 1984; *Forbes and Lin*, 2000). Thus, the electric field strength can be found using measurements of the velocity of the flare ribbons and the photospheric magnetic field. The evolution in time of this electric field during the flare gives the time profile of the reconnection rate (*Qiu et al.*, 2002).

Here, we use HXR footpoint sources as signatures of reconnection instead of Hα or UV ribbons because the HXR footpoint sources map to the main location of energy release (*Temmer et al.*, 2007, and references therin). Non-thermal HXR sources (above about 30 keV) are plausibly attributed to the locations where newly reconnected field lines intersect the chromosphere. Many cases of these HXR footpoint sources have been recorded over the last five years by the Reuven Ramaty High Energy Solar Spectroscopic Imager (RHESSI; *Lin et al.*, 2002).

To examine the topological location of magnetic reconnection, we use a magnetic charge topology (MCT) model in which point sources are located on the photospheric surface (see *Longcope and Klapper*, 2002). There are several advantages to this MCT method including: 1) Due to the fact that the topological features are quantitatively defined, powerful mathematical tools can be used. This includes the ability to calculate the magnetic flux linked by separators, which is employed in this Chapter. 2) The photospheric boundary of the model is a quantitative representation of the observed line of sight magnetogram. Model sources represent the flux and locations of sources in the magnetogram. The larger magnetic sources are represented by three poles, providing a quadrupolar expansion of these photospheric flux sources rather than a dipolar one. This allows us to examine internal

changes and rotations of sun spots (*Beveridge and Longcope*, 2006). 3) Calculation of the topological features of the model coronal field is not computationally time consuming, so we are able to study how the topology evolves over time.

For the reasons given above, we use a MCT model where the sources, or *poles*, are placed on the photospheric surface (see *Longcope and Klapper*, 2002). MCT models assume that the photospheric field can be partitioned into distinct unipolar regions. Also, they assume that any two field lines with both their footpoints in the same regions are topologically equivalent (*Longcope*, 2005). As a result of the first assumption, coronal field lines are anchored in discrete flux sources separated by a contiguous region in which the normal component of the magnetic field is zero. Each coronal field line can thus be assigned to a flux *domain* according to the poles at each of its two footpoints. *Nulls* are the locations between like signed poles where the magnetic field strength is zero. The surfaces dividing these domains are *separatrix* surfaces, which intersect along *separator* field lines. A separator is the three dimensional analog to a two dimensional X point; it is the location reconnection must occur in the three dimensional MCT coronal model.

There are two alternative methods to this MCT model that also give the topology of coronal magnetic fields: the source method (e.g. *Titov et al.*, 1993; *Demoulin et al.*, 1994; *Bagala et al.*, 1995; *Wang et al.*, 2002) and quasi-separatrix layers (QSLs; for a review see *Démoulin*, 2006). The source method represents the photospheric magnetic flux in a more complete way than is done in our model. For example, our method excludes the presence of magnetic bald patches successfully modeled by the source method. We are not, however, concerned with the modeling of bald patches, but are more interested in the powerful mathematical tools available through the use of the point-source MCT model. While our MCT method sacrifices a detailed representation of the coronal field, the calculation of QSLs *requires* its detailed structure as an input. The computation of this detailed structure is currently limited by numerical techniques. Thus, the current study of QSLs is limited to

a snapshot in time (*Démoulin*, 2006) and is not suitable for this work.

In this Chapter, we examine three flares that occurred within 30 degrees of disk center, were well observed by RHESSI, and had HXR footpoint sources that exhibited no motion. From Solar and Heliospheric Observatory/Michelson Doppler Imager (SOHO/MDI; *Scherrer et al.*, 1995) line-of-sight magnetograms we obtain the topology, and thus the separators, of the active region corona through extrapolation from the poles and nulls at the photospheric boundary. We measure the flux and length associated with each separator and derive a function related to the energy stored at them. This value is related to total self current, a current that acts to prevent flux changes and thus enables the field to increase its non-potentiality. We then use the function to identify the active region separators that have the most energy. In order to determine if a short interval of the continuous energy build up phase can point to the area of the active region in which the flare HXR footpoint emissions take place, we study a three hour time period prior to each of the flares.

The Chapter is organized as follows. In the Observations section, we discuss the HXR and magnetic field observations for the three flares in our study. Details of the analysis of the HXR footpoints and coronal topology as well as the results are given in Analysis and Results section. Finally, we give a discussion of the work in the Discussion and Conclusions section.

Observations

The flares that we have analyzed in this study were chosen because they fulfill the three requirements stated above. The requirement that the flares must have occurred within 30 degrees of disk center is motivated by the fact that line of sight magnetic field beyond this range is not sufficiently close to the normal field used in the topology calculation. Secondly, the flares needed to be well observed by RHESSI so that we could make resolved images of the footpoints sources as well as be confident about the flare's basic morphology over its

lifetime. For this study, we chose flares whose footpoints did not move because we wanted to be able to associate flares and separators without introducing undue complexity. The properties of the three flares are given in Table 4.1.

The two most commonly used RHESSI image reconstruction algorithims are Clean (*Högbom*, 1974; *Hurford et al.*, 2002) and Pixon (*Puetter*, 1995; *Hurford et al.*, 2002). Clean is an iterative reconstruction algorithm that is quick and often satisfactorally represents both point and extended sources. For these reasons, we used Clean to make the images analyzed in flares B and C. Occasionally, the Clean algorithm does not remove enough noise from an image such that the morphology of the sources is not clear. In some of these cases, the Pixon algorithm, which has superior noise reduction and photometry, can result in an image with sufficently defined sources. While Pixon gives superior images, it is significantly more time consuming than Clean. For this reason, it is typically not the first choice for exploring HXR sources observed by RHESSI. Due to the low number of counts available for making an image of the footpoints of flare A, the two sources could not be distinguished from one another at the 30% level of the Clean image. Therefore, we use a Pixon image in this case.

The first flare, hereafter flare A, occurred on 26 February 2004. As can be seen in Figure 4.1, this flare was a *GOES* X1 class flare that had an impulsive phase lasting only a few minutes. The small peak in the RHESSI 50-100 keV emission around 01:54:30 UT is the only time it was possible to make an image of the HXR sources in this energy range. Detailed spectroscopic analysis of the flare has shown that the 25-50 keV counts after about 01:58 UT are primarily thermal in nature. The contours used to classify the flaring separators for flare A are drawn at the 20% level of a 30-100 keV Pixon image. The image, shown in Figure 4.2, was made by summing the counts in detectors 1-9 from 01:54:40-01:55:00 UT in the 30-100 keV range.

The second flare, hereafter flare B, took place on 6 April 2004. Flare B, an M2 class

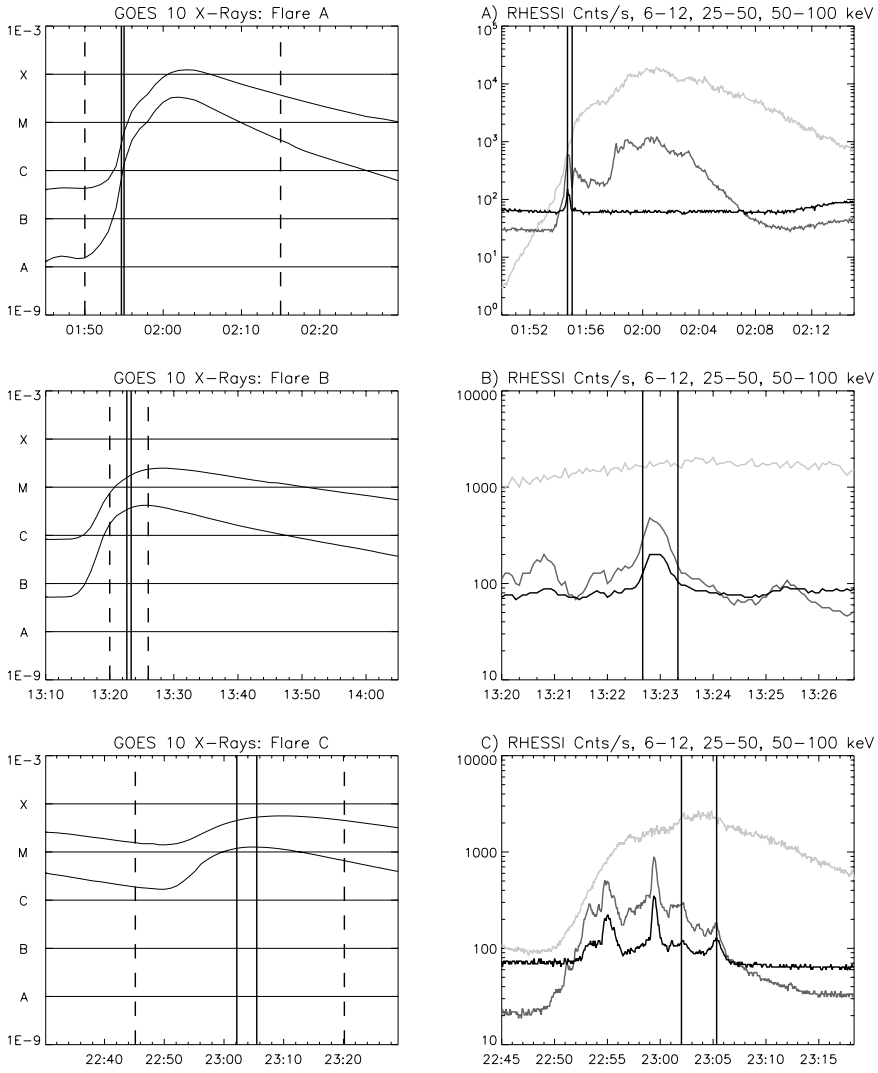

Figure 4.1: GOES and RHESSI light curves. Dashed lines in the left panels mark the time range for the right panels. The right hand panels are corrected RHESSI light curves, where the effects of attenuator and decimation state changes are accounted for. The 6-12 keV curves are light grey, 25-50 keV are dark grey and 50-100 keV are black. Solid vertical lines mark the time range over which the RHESSI images used in Figures 4.2 and 4.3 were integrated.

Table 4.1: Flare properties.

Flare	Date	Location (heliocentric ″)	Peak Time (UT)	*GOES* Class	AR
A	26 Feb 2004	(230,330)	02:01	X1	10564
B	6 Apr 2004	(-260, -180)	13:23	M2	10588
C	4 Nov 2004	(-280,70)	23:02	M5	10696

flare, was a typical mid-sized flare with a single X-ray loop and an impulsive phase lasting on the order of 10 min. The image used here was made with the Clean algorithm by summing the HXR counts in detectors 4-8 from 13:22:40-13:23:20 UT in the 25-50 keV energy range. The contours used to identify the flaring separators were defined at 30% of the maximum of this image.

The third flare, hereafter flare C, took place on 4 November 2004. Flare C was a long duration M5 class flare with an impulsive phase of about 17 min. It occurred to the West of another M class flare that peaked an hour earlier in the same active region. During the second half of the impulsive phase, a third 25-50 keV HXR source appeared to the Northeast of the primary pair. Our hypothesis for the appearance of this third HXR source is discussed in the Discussion and Conclusions section. The image used in our analysis was made with the Clean algorithm by summing the HXR counts in detectors 4-8 from 23:02:00-23:05:20 UT in the 25-50 keV range. The contours used to identify the flaring separators were defined at 30% of the maximum of this image.

Based on MDI magnetograms, we calculate the topology of the coronal field based on full disk MDI magnetograms three times for each flare, two prior to the flare and one after. For flare A, which peaked at 02:01 UT, the magnetic field data were taken in 96 min. intervals at 00:03, 01:39 and 03:15 UT. The magnetograms for flare B, which peaked at 13:23 UT, were made at 11:11, 12:51 and 14:27 UT. Around the time of flare C, which peaked at 23:02 UT, MDI magnetograms were taken every minute. We noticed that subtle changes were present in data taken just one minute apart, which we attributed to noise. In

order to take advantage of the available data while decreasing the noise level, we averaged five consecutive one-minute magnetograms at 21:14-18, 22:14-18 and 23:15-19 UT. This technique of averaging over five one min. magnetograms is the same as is done on-board the spacecraft for the 96 min. magnetograms, which are used in flares A and B.

We took a straight-forward approach to the co-alignment of the MDI magnetograms and RHESSI data. *Fletcher et al.* (2007) report that the difference in the roll angle given in the MDI data files and the actual roll averages around 0.22 degrees, which corresponds to a combined *x*-*y* offset of $3''$ at the limb. However, we have proceeded on the assumption that the roll angle is 0 (rotated from 180 degrees in the case of flare A) and that the spatial alignment of MDI data, corrected to Earth view, and RHESSI data taken at the same time agree to within $2''$ (*Krucker et al.*, 2005). The RHESSI data were differentially rotated to the time of the MDI observations using the SolarSoft mapping software developed by D. Zarro. While the mapping software is an approximation to the actual rotation, it is suitable for our purposes as we did not require a rotation correction of more than $\sim$2.5 hours.

Analysis and Results

Our analysis of the topological location of magnetic reconnection proceeds under the following working hypothesis. In the absence of reconnection, coronal magnetic fields become stressed as the photospheric boundary slowly evolves due to the emergence of new field and horizontal flows. When a critical point is reached, this energy is released by the rapid reconnection of magnetic field lines near the separator. As a result, electrons are accelerated near the reconnection region and stream along field lines near the separator. Upon encountering the chromosphere, the electrons undergo bremsstrahlung and non-thermal HXR are emitted. Thus, HXR footpoint sources can be interpreted as the location of the chromospheric ends of newly reconnected field lines, which lie close to the separator.

In order to make the connection between a flare's reconnection region and its HXR footpoints, we need to define the separators. We determine the connectivity of the field by making a model of the active region's photospheric sources observed in MDI line-of-sight magnetograms. The observed field is partitioned by grouping pixels that exceed a set threshold (100 G for flares A and B, 75 G for flare C) and are downhill from a local maximum. Regions with fewer than 10 pixels are deemed to be energetically unimportant and are discarded. Each source region with a flux less than 5×10^{19} Mx is characterized by a single point source, or pole, which matches the region's net flux and is located at the region's flux centroid. Regions with fluxes greater than 5×10^{19} Mx are represented by three poles, each with 1/3 of the region's flux, placed such that their centroid is at the same location as the region's and their quadrupole moment matches the region's. The quadrupolar expansion enables the observation of internal changes and rotations of large regions and decreases the uncertainty in the locations of topological features. A potential field extrapolated from these poles determines the locations of the topological features of the field including nulls, separatricies and separators.

As with any coronal field extrapolation model currently available, there are limitations to the MCT model we use. One limitation of our model is the loss of information on the geometry of the field. This is a result of representing patches of magnetic field with point sources. While using three point sources for the larger patches decreases the spatial uncertainty in the model, we still cannot distinguish if a coronal field line emanates from the outside edge of the modeled source or the center, for example. Another limitation of this extrapolation model is that it is potential. Currently, we do not have the ability to model coronal fields above the complex active regions where flares typically occur with a non-linear force free field model. A moderately stressed field, however, has a topology similar to that of the potential field (*Brown and Priest*, 2000); it has the same separators dividing the flux domains. A third limitation of this MCT model is our inability to consider open

field lines or sheared or twisted flux tubes, whose currents can induce significant topological changes. This means that we cannot say anything about the properties of the field at the moment of the flux tube eruption in the CSHKP model. We can, however, examine the closed field prior to and after the flare. The evidence we have for reconnection deals with electrons streaming along the closed field lines that have collapsed down beneath the separator. Using these closed field lines and the information we have from HXR emission still allows us to point to the topological location of reconnection and thus learn a great deal about the storage and release of energy in flares.

When using flare footpoints as a signature of reconnection in the corona, one of the first steps is to establish footpoint conjugacy. We have done this using three techniques. First, we compare the general characteristics (e.g. rise, peak and decay times) of the HXR light curves of the candidate pair. If the two footpoints are connected by the same field lines, then the fast electrons running down either side of those lines should impact the chromosphere within one second of each other. Second, we examine the topology model to see if a connection exists between the positive and negative magnetic sources associated with the footpoints. Third, we look for a bright soft X-ray or extreme ultraviolet loop connecting the HXR source regions. This visual connection gives credence to hot evaporated plasma having filled up the newly reconnected loop. The main HXR flare footpoints for the three flares fulfill each of these conjugacy tests, so we conclude that the HXR sources used in the analysis of flares A, B and C are conjugate.

Once the separators of each flaring active region have been determined, is there evidence that energy was stored preferentially at the flaring separators prior to the flare? To answer this question, we first identified all of the separators we believed to be involved in the release of energy via reconnection based on our observational criteria. These flaring separators were assumed to be those that had both their ends within $10''$ of the defined HXR footpoint contours. We use the $10''$ extension on the footpoint contours because of

the uncertainty in the locations of the chromospheric ends of the separators (nulls). When representing the larger magnetic field sources with three poles, as we do here, the typical distance between nulls is $\sim 10''$.

In order to have a precise estimate of the energy stored at every separator, we attempted to follow each individual separator by matching its nulls at one time to the next. We found, however, that we were unable to complete our analysis using only the separators we could identify as the same in consecutive topology calculations. Only a small number of separators were followable because the majority of the separators that we examined bifurcated. A bifurcation is when a separator that is present at one time is not present at the next (or vice versa). With only a small number of separators, we were not able to represent the various parts of the active region well enough to obtain meaningful energy estimates.

Since we were not able to follow individual separators directly, we grouped the separators into null group pairs (NGPs). We partitioned areas of the analyzed MDI magnetograms into null groups (NGs) such that the NG areas corresponded as closely as possible to areas of strong magnetic flux while keeping all the nulls at the ends of the flaring separators in the same NG. Every separator begins and ends at a null point and thus can be categorized by its two NGs, or its NGP. Figure 4.2 shows the poles, nulls and null groups as well as the footpoint contours of the three flares on the corresponding magnetograms. The use of NGPs has a further advantage over following each individual separator in that it is less biased. Using only the followable separators is biased because it ignores bifurcated separators, which are indicators of major change.

Having categorized the separators into null group pairs, we were able to analyze the separators belonging to the flaring NGPs with respect to the non-flaring ones. We sought to determine if there is evidence for energy being stored preferentially at the flaring separators. Also, we wanted to ascertain if a small time sample ($\sim$3 hours) could serve as a proxy for the changes taking place over the longer energy build-up phase prior to the flare.

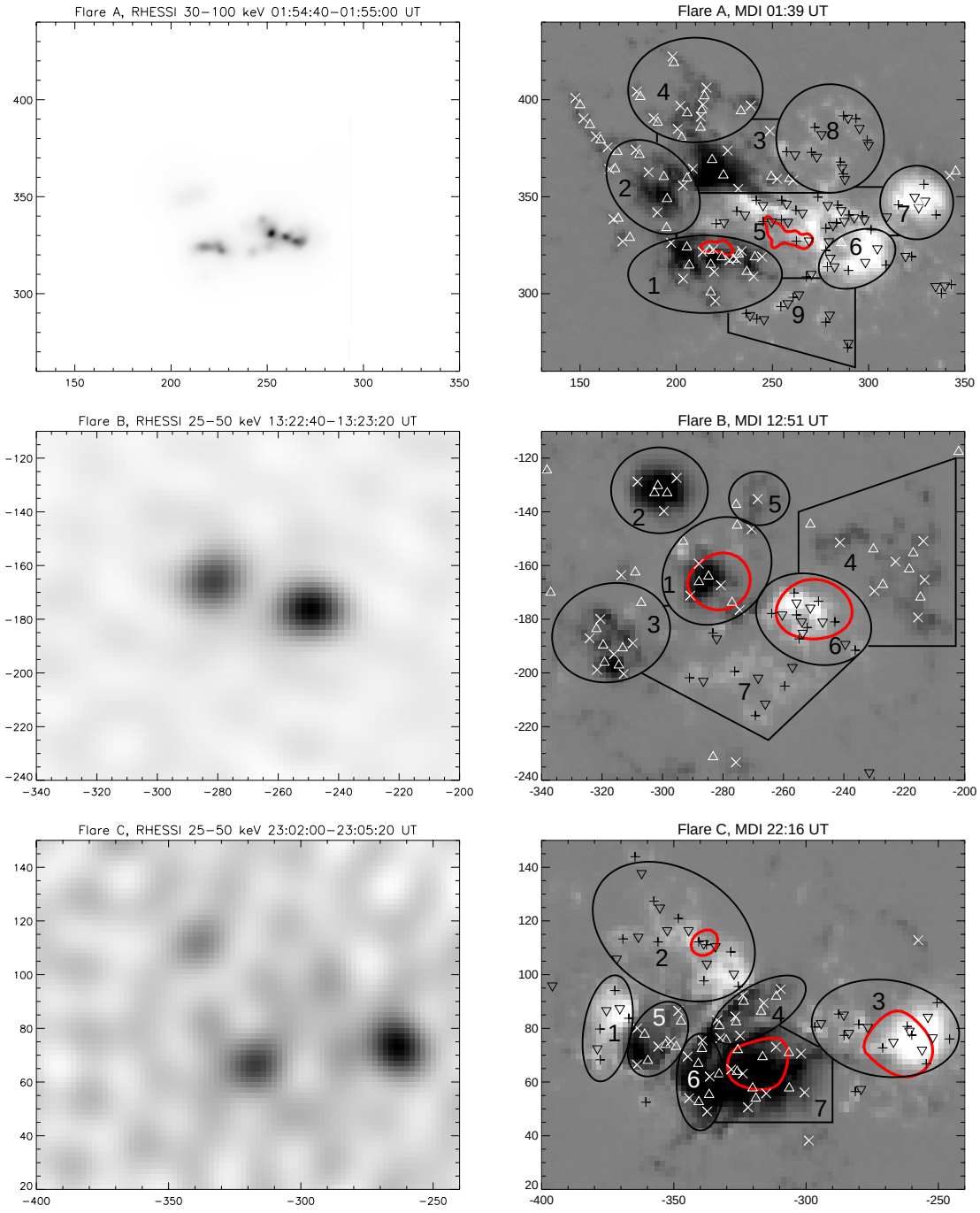

Figure 4.2: Left panels: RHESSI images used in our analysis. Right panels: MDI magnetograms with poles (+ positive, × negative), nulls (▽ positive, △ negative), null groups (outlined in black) and footpoint contours (red). Footpoint contours are at the 20% level of a 30-100 keV RHESSI Pixon image for flare A and at the 30% level of 25-50 keV RHESSI Clean images for flares B and C.

To do this, we measured the flux, $\Phi^{(\mathrm{v})}$, that interconnects photospheric sources by integrating the vector potential along the path *Q* (*Longcope et al.*, 2005),

$$\Phi^{(\mathrm{v})} = \int_S \boldsymbol{B} \cdot d\boldsymbol{a} = \oint_Q \boldsymbol{A} \cdot d\boldsymbol{l}. \tag{4.1}$$

Here, *Q* is the separator field line closed along the photosphere and *S* is some surface bounded by *Q*. We calculated this flux for every separator obtained by the model from three consecutive 96 minute MDI magnetograms, or from three averaged magnetograms one hour apart in the case of flare C. As an example, we consider null groups 3 and 7 of flare C, located in the lower right of the active region image in Figure 4.3. The separators connecting these null groups, shown in red, have the average flux 29 $\times 10^{11}$ Tm^2 at this time (22:16 UT). At times before and after, 21:16 and 23:17 UT, separators in the same null group averaged 12 $\times 10^{11}$ and 25.5 $\times 10^{11}$ Tm^2 respectively. We also measure the average length, l_s, of the separators in every NGP at each of the three times. The average length of the separators in NGP 3,7 of flare C at the time shown was 46 $\times 10^6$ m, and was 34 $\times 10^6$ m at the previous time, 21:16 UT and 68 $\times 10^6$ m at the following time, 23:17 UT.

We relate this flux to the energy stored at the separators by assuming that the continually changing *photospheric* magnetic field (and thus the change in separator flux) translates into a storage of energy in the *coronal* field. The flux Φ_r reconnected during the flare can be approximated as the discrepancy between the flux *actually* linked by the separator, Φ_s, and the flux linked by it in a potential field, $\Phi_s^{(\mathrm{v})}$. Prior to reconnection the flux discrepancy Φ_r = Φ_s - $\Phi_s^{(\mathrm{v})}$ changes only due to the slow, steady change in $\Phi_s^{(\mathrm{v})}$:

$$\frac{\mathrm{d}}{\mathrm{d}t}\Phi_r = -\frac{\mathrm{d}}{\mathrm{d}t}\Phi_s^{(\mathrm{v})}. \tag{4.2}$$

Photospheric stressing persisting steadily over a build-up time Δt_b then would build up a

flux discrepancy

$$\Delta\Phi_r = -\Delta t_b \frac{\mathrm{d}}{\mathrm{d}t}\Phi_s^{(\mathrm{v})} \simeq \Delta t_b E_b l_s, \tag{4.3}$$

where l_s is the length of the separator. The quantity

$$E_b \simeq -(\mathrm{d}\Phi_s^{(\mathrm{v})}/\mathrm{d}t)/l_s \tag{4.4}$$

is one measure of how rapidly stress is building on a particular separator. It has units of electric field, but there is no electric field present during energy build-up. During reconnection, energy stored in the form of the flux discrepancy is released in the presence of an electric field, E_r over a time period Δt_r. This reconnection electric field is related to Φ_r by

$$\frac{\Delta\Phi_r}{\Delta t_r} = -E_r l_s. \tag{4.5}$$

Thus the separator stress, E_b, is related to the reconnection electric field by

$$E_r = \frac{\Delta t_b}{\Delta t_r} E_b. \tag{4.6}$$

Since we do not observe the active region over its entire build-up, we do not know Δt_b or Φ_r. We can, however, use observations over a short interval Δt to estimate the separator stress

$$E_b \simeq -\frac{1}{l_s}\frac{\Delta\Phi_s^{(\mathrm{v})}}{\Delta t}. \tag{4.7}$$

Continuing with the above example, NGP 3,7 of flare C, we find that the change in average separator flux, $\langle\Delta\Phi_s^{(v)}\rangle$, from 21:15 to 22:15 UT was 17 $\times 10^{11}$ Tm^2 and the average length, $\langle l_s\rangle$, was 40 $\times 10^6$ m. When we divide $\langle\Delta\Phi_s^{(v)}\rangle$ by $\langle l_s\rangle$ and Δt = 3600 s, we find that $\langle E_b\rangle \simeq 12$ Vm^{-1}. Values of $\langle E_b\rangle$ for the NGPs of flares A, B and C are given graphically in Figure 4.3 and numerically in Table 4.2. In the table, E1 is the value of $\langle E_b\rangle$ calculated

Table 4.2: Values of the separator stress $\langle E_b \rangle$. Units of $\langle E_b \rangle$ are V m^{-1}. Null Group Pairs are labeled in Figures 4.2 and 4.3. Ave is the average of the two measured values of $\langle E_b \rangle$. The * indicates the flaring null group pairs.

Flare A NGP	E 1	E 2	Ave	Flare B NGP	E 1	E 2	Ave	Flare C NGP	E 1	E 2	Ave
1,5*	0.73	4.91	2.82	1,6*	2.90	2.73	2.82	1,5	8.14	1.39	4.76
1,6	0.40	0.87	0.64	3,7	2.27	0.64	1.46	2,4	0.36	0.39	0.38
1,9	0.02	0.78	0.40	4,6	0.31	0.82	0.57	2,5	2.97	1.08	2.03
2,5	8.65	2.76	5.71	4,7	1.39	1.60	1.50	2,6	2.08	1.86	1.97
3,5	0.42	4.36	2.39					2,7*	0.72	4.53	2.63
4,8	0.35	0.17	0.26					3,7*	12.00	1.89	6.94

from differences in the first and second set of separators and E2 is from differences in the second and third.

For each flare, we have measured $\langle E_b \rangle$ for every null group pair that has at least three separators in all three analyzed topologies. (This choice is somewhat arbitrary. However, the same set of NGPs would be analyzed if we chose the NGPs with at least two separators.) We do not analyze separators that appear in groups of two or less because the average change in flux can be completely dominated by the bifurcation of a single separator. While bifurcations are good indicators of where major change is occurring in the active region, they result in incomparable flux changes when there are only one or two separators in a group to average over. We also do not consider separators that have one or both ends at nulls that do not belong to any NG.

In Figure 4.3, we have plotted the nulls and separators of the calculated topology from the middle time analyzed in each flare, 01:39, 12:51 and 22:14-18 UT for flares A, B and C respectively. The group of separators shown in red in each of the panels of Figure 4.3 are those that had the largest separator stress$\langle E_b \rangle$. For flares B and C, the group of separators that had the largest $\langle E_b \rangle$ were the separators that were associated with the HXR footpoint sources and thus with magnetic reconnection. In the case of flare A, the largest $\langle E_b \rangle$ was not measured in the flaring NGP 1,5, but in NGP 2,5. The flaring NGP did, however, exhibit

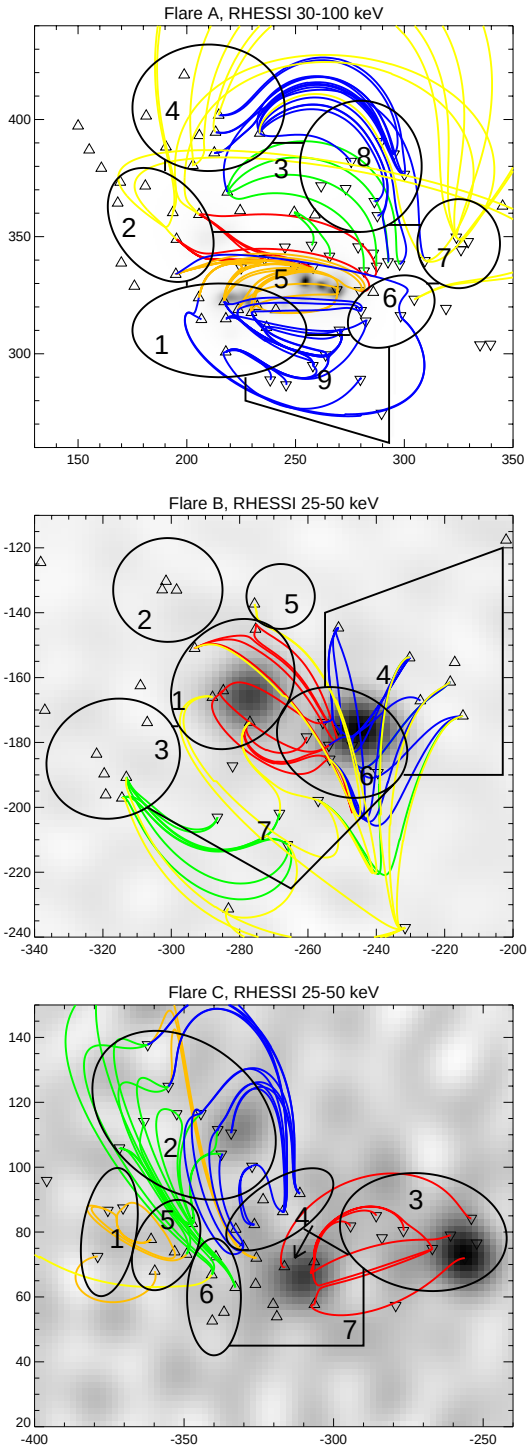

Figure 4.3: RHESSI images with null groups and separators. Separators are color coded according to average E_b, where red indicates the largest $\langle E_b \rangle$ in each flare: red = above 5 V m^{-1} (except in the case of flare B where red = above 2.5 V m^{-1}), orange = between 2.5 and 5 V m^{-1}, green = between 1 and 2.5 V m^{-1}, blue = below 1 V m^{-1} and yellow = separators not considered (see the Analysis and Results section for details).

the second largest $\langle E_b \rangle$.

In order to quantify the significance of this result, we found the probability of having one of the top two best outcomes in the relationship between flaring NGP and the value of$\langle E_b \rangle$, the best outcome being that the flaring NGPs had the largest $\langle E_b \rangle$in all three flares. Our result is the second best outcome, with two of the flares having the largest $\langle E_b \rangle$ and the third flare having the second largest. Out of 144 possible outcomes ($6 \times 4 \times 6$ NGPs for flares A, B and C, respectively), there is one way of having the best outcome and three ways of having the second best. Thus, there is a 4/144 or ~2.8% chance of having one of the top two best outcomes. Therefore, we find that the statistical significance of this result is ~97.2%. The actual situation, however, is more clear-cut than the 97% confidence implies. In the two cases where the flaring NGP has the largest $\langle E_b \rangle$, this value is a clear outlier; it is larger than the next highest value by 46 and 30% for flares B and C.

Discussion and Conclusions

We conclude that we are able to understand the location of HXR sources observed in flares in terms of a physical and mathematical model of the topology of the flaring active region. In this Chapter, we have calculated the fluxes and lengths of the separators present in three flaring active regions based on MDI magnetograms and a MCT model. We studied the change in average separator flux per unit length, $\langle E_b \rangle$, where the average was over the separators belonging to the same null group pair. The function $\langle E_b \rangle$ is proportional to the self current that acts to prevent flux changes in the coronal field and is thus a signature of non-potentiality and energy storage. We find that the separator stress, $\langle E_b \rangle$, is largest for the flaring null group pair in two of the flares and is second largest in the third flare. Thus, we have shown that separators connecting the HXR sources of these flares are highly stressed.

This conclusion supports the hypothesis that the energy associated with reconnecion

(in the form of heating and particle acceleration) is released near separators. Prior to a flare, energy is built up in the stressed coronal field due to motions in the photospheric field. During a flare, this energy is released via reconnection at separators, resulting in the acceleration of electrons on field lines near the separator. The electrons stream along these field lines until they encounter the chromosphere and emit HXR.

In this Chapter, we implicitly assume that the numerical technique we use to calculate separators locates them all each time. When we attempted to follow each individual separator by matching their nulls from one time to the next, we found that a majority of the separators could not be followed. This means that either there are many separator bifurcations or our assumption about the separator locating method is not correct. We are not sure what percentage of the currently observed separator bifurcations are real and not an artifact of noise. Work is currently being done to better understand the separator locating technique.

As an example of what we consider to be real separator bifurcation, we consider the topology shown in Figure 4.3 for flare C. This topology does not have a separator connecting from the middle HXR source to the third footpoint (located in NG 2) which is present in the second half of flare C's impulsive phase. Several separators, however, connect the two sources in the previous and following times (at 21:15 and 23:15 UT). The bifucation of these separators suggests a major change taking place in this area of the photospheric field, which causes the build up of stress in the coronal field above it. These connecting separators are linked to a common null (shown by the arrow) shared by the northern most flaring separator in NGP 3,7. We suggest that the third footpoint appeared because the reconnection which started on the NGP 3,7 separators triggered a secondary reconnection event, via the common null, to release energy stored at the NGP 2,7 separators.

We also conclude that the relative value of separator stress, measured for a period of time as short as 2 hours, can be used as an indicator of where within an active region

a major flare is likely to occur. For the three flares studied here, which are among the largest produced by thier active regions, we found that reconnection occurred at strongly stressed separators. Even in the case of flare A, which is superficially different in that more energy went into heating rather than particle acceleration, the separators of the flaring NGP were highly stressed compared to all but those in one other NGP. Hence we conclude that topological methods have the potential to reveal possible sites of major flares.

CHAPTER 5

DISCUSSION AND CONCLUSIONS

Summary and Conclusions

In this dissertation, I combine the analysis of HXR footpoint sources with a 3D topology model in order to further the understanding of the evolution and location of magnetic reconnection in solar flares. I assume that a solar flare releases energy, in the form of heating and particle acceleration, from stressed coronal fields via reconnection at special field lines called separators. Separators are topological features that I define by a simple but quantitative model of the flaring active region's magnetic field. Imbalances in the magnetic flux of highly stressed regions of the coronal field determine the location and evolution of reconnection. The process of reconnection acts to accelerate charged particles that then stream along newly reconnected field lines near the separator until they encounter the chromosphere, where their kinetic energy is converted into HXR. Thus, by combining HXR observations and a magnetic topology model I can determine the location and evolution of reconnection.

The HXR sources I examined in this study were observed by RHESSI. The RHESSI instrument was ideal for this work because I was able to identify and image HXR footpoint sources with high positional and temporal resolution. Electrons accelerated during reconnection stream along both sides of newly formed field lines just under the reconnection region until they encounter the chromosphere and convert their energy into HXR footpoint sources. Thus, I use HXR footpoint sources observed by RHESSI as signatures of magnetic reconnection.

This magnetic reconnection is believed to take place near separators, which I define

with a magnetic charge topology (MCT) model. The MCT model quantitatively characterizes the 3D connectivity of the magnetic field, which is helpful in this study because it allows for the use of powerful mathematical tools such as relating HXR footpoint motions to the transfer of magnetic flux during separator reconnection and identifying the main locations of energy build-up in active region magnetic fields. Therefore, while this study could have been done using other observational and topological methods, I have shown that I can explain the location and evolution of reconnection using RHESSI data and a MCT model.

In Chapter 2, I analyzed the relationship between HXR footpoint motions and spine lines in three flares. Spine lines, which extend from a pole through a null to another pole of the same polarity, are the topological characterization of extended regions of like flux. It is not surprising, therefore, that the HXR footpoints move along the spine lines. I found that I could reject the hypothesis that the average spine line and footpoint track angles have a random relationship with 99.95% confidence.

This association between HXR footpoint tracks and spine lines cannot be predicted by the standard 2.5D flare model. Thus, I explain this association using a simple quadrupolar footpoint model, which is an evolution of the standard 2.5D model into 3D. The simple configuration is not meant to model the entire flaring region, but rather, the separator in the configuration is one of several on which reconnection occurs over the course of a flare.

I discussed three cases of reconnection events for this footpoint motion model. In each case, reconnection acts to correct an imbalance of flux in the configuration. This reconnection takes place on a separator, changing the morphology of the separator in the process. Changes in the location of the chromospheric ends of the separator result in 'movement' of HXR sources because the fast electrons accelerated during reconnection stream along field lines near the separator until they encounter the chromosphere where some of their kinetic energy is converted into HXR emission. The movement of the chromospheric ends of the

separator (nulls) are along spine lines because spine lines connect like sources via a null between them; as the amount of flux in each domain shifts, the associated nulls move along this line.

The footpoint motion model presented in Chapter 2 explains not only why HXR sources move along spine lines, but why three types of relative HXR footpoint motion are commonly observed: anti-parallel with decreasing separation, anti-parallel with increasing separation and parallel with little change in separation. Thus, the model can be compared to other models that have been proposed to explain HXR footpoint motion (and thus reconnection), which can lead to a better understanding of the flare process.

All topological features are determined by the way the photospheric sub-region magnetic flux sources are represented in a topology model. Work in the course of this thesis revealed that in order to fully understand RHESSI observations, it was necessary to introduce a more complete representation of the magnetic polarities than the one used in the original MCT method. In Chapter 3, I described the method I used to define the more detailed representation, which replaces the sub-region magnetic flux sources observed in magnetograms with a multipole expansion out to the third (quadrupole) term. I also compared the topological features produced by the original method, which replaces the sub-regions with an expansion out to the second (dipole) term, to the new method in two cases: a simple simulated magnetogram and a real magnetogram of a flaring active region.

I found that the new quadrupole method, which produces nulls and separators internal to sub-region sources, can be used to model reconnection resulting from internal changes and rotations of strong photospheric flux regions while the original method cannot. This photospheric shearing is thought to be one of the main ways energy is built-up in coronal fields. Therefore, the new quadrupole expansion method is used in my study of the location of magnetic reconnection, described in Chapter 4.

In Chapter 4, I examined the build-up of energy prior to three flares as indicated by

changes in the active region separators. Prior to a flare, continuous changes in the photospheric boundary of an active region's line-tied magnetic field set the chromospheric and coronal plasma in motion. Due to the lack of major reconnection in the corona, these changes build up the free energy needed to power a flare. The field becomes more and more stressed as the energy builds until some critical point is reached and a flare occurs, releasing the energy and returning the corona to a lower energy state.

In this study, I measured the flux and length associated with each separator and derived a function related to the energy stored at them. This value, separator stress, is related to total self current, which acts to prevent flux changes and thus enables the field to increase its free energy. I used the separator stress to determine if there is evidence for energy being stored preferentially at the flaring separators (those connecting HXR footpoint sources). I found that the separator stress was largest for the flaring separators in two of the three flares and second largest in the third flare.

This result shows that separators connecting HXR sources of the three major flares examined here are more highly stressed than most of the other separators in the active region. This suggests that the study of the separators given by the MCT model can indicate where within an AR a flare is likely to occur.

In summary, based on the success of the MCT model in relating the motion of HXR sources to the evolution of magnetic reconnection on coronal separators, as well as my mathematical and physical model of energy storage at separators, I conclude the MCT model gives useful insight into the relationship between sites of HXR emission and the topology of flare productive active regions.

Future Work

The Rarity of HXR Ribbons

Comparison of HXR sources with Hα and UV images shows that most often the HXR

emission is concentrated in compact sources that cover only a small part of the Hα and UV flare ribbons. The 2D standard flare model predicts that HXR sources should be analogous to flare ribbons, but observational evidence suggests that the correlation does not hold in 3D. The analysis of coronal magnetic topology in the context of flare HXR footpoint sources can give insight into why the number of HXR ribbons relative to Hα and UV flare ribbons is so low.

There are two scenarios that can account for the lack of HXR ribbon sources (*Temmer et al.*, 2007). (1) Chromospheric HXR emission is solely due to precipitating electrons accelerated along a small subset of loops, whereas Hα and UV emissions can be excited by electron bombardment and other processes, such as heat flux from the hot flaring corona (see e.g. *Fletcher and Hudson*, 2001). (2) The limited dynamic range of X-ray instruments may lead to the effect that only the strongest nonthermal sources are observed in HXRs and weaker ones are buried in the noise of the instruments. Even if scenario 2 is correct, however, the question remains: Why is a portion of the footpoint source always strong enough to drown out the weaker parts, exceeding the weak portions by a factor of at least ten in the case of RHESSI observations?

The technique used in Chapter 4 to examine the build-up of energy prior to a flare can be used to study the morphology of HXR sources compared to Hα and UV ribbons. I hypothesize that the separators connecting HXR sources within the flare ribbons have greater separator stress than the separators connecting the two flare ribbons but not HXR sources. This study can be done in the same basic way as was done for the three flares in Chapter 4; the only difference being the need to select the null groups more precisely such that there is a clear distinction between separators connecting HXR sources and those not.

Signatures of Energy Build-up and Release

While there are many studies that examine the evolution of flares, the question of why

they occur where and when they do is much more challenging and speculative. Past research on flare energy build-up and release has concentrated on nonpotential signatures in vector magnetograms (i.e. *Gary et al.*, 1987; *Wang et al.*, 1996; *Moon et al.*, 2000; *Deng et al.*, 2001; *Tian et al.*, 2002; *Dun et al.*, 2007). For example, *Dun et al.* (2007) calculated the daily average values of three nonpotential parameters from vector magnetograms of selected regions along the main neutral lines of active region 10486. They found that the three non-potentiality parameters increased at the impulsively brightening flare sites from values measured at least one day before the two large X-class flares of 28 and 29 October, 2003. While most of the measured parameters decreased after the flares, as expected due to the relaxation of nonpotentiality, some continued to increase. This and other, similar studies indicate that more research is required to fully understand the relationship between observational signatures of nonptentiality and the build-up and release of energy in flaring active regions.

The results given in Chapter 4 of this dissertation show that there is preferential stressing at flaring separators in the few hours prior to a flare. This stressing is related to build-up of nonpotentiality in the active region magnetic field. Just as the nonpotential signatures examined in vector magnetograms have been shown to increase prior to a flare and decrease afterward (e.g. *Wang et al.*, 1996), the temporal evolution of separator stress in the *tens of hours* prior to a flare may give clues to flare occurrences. The added benefits of the separator stress method are that it can be done using line-of-sight magnetograms, which are more readily available, and that it deals with 3D coronal features rather than chromospheric ones. Therefore, it is possible that the topological methods I developed in this dissertation offer a mathematical and physical method for examining why flares occur when they do.

REFERENCES

Aulanier, G., P. Démoulin, B. Schmieder, C. Fang, and Y. H. Tang, Magnetohydrostatic Model of a Bald-Patch Flare, *Sol. Phys.*, *183*, 369–388, 1998.

Aulanier, G., E. Pariat, P. Démoulin, and C. R. Devore, Slip-Running Reconnection in Quasi-Separatrix Layers, *Sol. Phys.*, *238*, 347–376, 2006.

Bagala, L. G., C. H. Mandrini, M. G. Rovira, P. Demoulin, and J. C. Henoux, A Topological Approach to Understand a Multiple-Loop Solar Flare, *Sol. Phys.*, *161*, 103–121, 1995.

Beveridge, C., and D. W. Longcope, A Hierarchical Application of the Minimum Current Corona, *ApJ*, *636*, 453–461, 2006.

Bogachev, S. A., B. V. Somov, T. Kosugi, and T. Sakao, The Motions of the Hard X-Ray Sources in Solar Flares: Images and Statistics, *ApJ*, *630*, 561–572, 2005.

Brown, D. S., and E. R. Priest, Topological differences and similarities between force-free and potential models of coronal magnetic fields, *Sol. Phys.*, *194*, 197–204, 2000.

Brueckner, G. E., R. A. Howard, M. J. Koomen, C. M. Korendyke, D. J. Michels, J. D. Moses, D. G. Socker, K. P. Dere, P. L. Lamy, A. Llebaria, M. V. Bout, R. Schwenn, G. M. Simnett, D. K. Bedford, and C. J. Eyles, The Large Angle Spectroscopic Coronagraph (LASCO), *Sol. Phys.*, *162*, 357–402, 1995.

Carmichael, H., A Process for Flares, in *The Physics of Solar Flares*, edited by W. N. Hess, pp. 451–+, 1964.

Démoulin, P., Extending the concept of separatrices to QSLs for magnetic reconnection, *Advances in Space Research*, *37*, 1269–1282, 2006.

Demoulin, P., C. H. Mandrini, M. G. Rovira, J. C. Henoux, and M. E. Machado, Interpretation of multiwavelength observations of November 5, 1980 solar flares by the magnetic topology of AR 2766, *Sol. Phys.*, *150*, 221–243, 1994.

Demoulin, P., L. G. Bagala, C. H. Mandrini, J. C. Henoux, and M. G. Rovira, Quasi-separatrix layers in solar flares. II. Observed magnetic configurations., *Astronomy and Astrophysics*, *325*, 305–317, 1997.

Deng, Y., J. Wang, Y. Yan, and J. Zhang, Evolution of Magnetic Nonpotentiality in NOAA AR 9077, *Sol. Phys.*, *204*, 11–26, 2001.

Des Jardins, A. C., R. C. Canfield, D. W. Longcope, C. Fordyce, and S. Waitukaitis, Reconnection in Three Dimensions: The Role of Spines in Three Eruptive Flares, *ApJ*, *submitted*, 2007a.

Des Jardins, A. C., R. C. Canfield, D. W. Longcope, E. McLinden, and A. Dillman, Signatures of Magnetic Stress Prior to Three Solar Flares Observed by RHESSI, *ApJ*, *accepted*, 2007b.

Dun, J., H. Kurokawa, T. T. Ishii, Y. Liu, and H. Zhang, Evolution of Magnetic Nonpotentiality in NOAA AR 10486, *ApJ*, *657*, 577–591, 2007.

Falconer, D. A., R. L. Moore, and G. A. Gary, Magnetic Causes of Solar Coronal Mass Ejections: Dominance of the Free Magnetic Energy over the Magnetic Twist Alone, *ApJ*, *644*, 1258–1272, 2006.

Fletcher, L., and H. Hudson, The Magnetic Structure and Generation of EUV Flare Ribbons, *Sol. Phys.*, *204*, 69–89, 2001.

Fletcher, L., and H. S. Hudson, Spectral and Spatial Variations of Flare Hard X-ray Footpoints, *Sol. Phys.*, *210*, 307–321, 2002.

Fletcher, L., I. G. Hannah, H. S. Hudson, and T. R. Metcalf, A TRACE White Light and RHESSI Hard X-Ray Study of Flare Energetics, *ApJ*, *656*, 1187–1196, 2007.

Forbes, T. G., and J. Lin, What can we learn about reconnection from coronal mass ejections?, *Journal of Atmospheric and Solar-Terrestrial Physics*, *62*, 1499–1507, 2000.

Forbes, T. G., and E. R. Priest, Numerical simulation of reconnection in an emerging magnetic flux region, *Sol. Phys.*, *94*, 315–340, 1984.

Foukal, P. V., *Solar Astrophysics, 2nd, Revised Edition*, Solar Astrophysics, 2nd, Revised Edition, by Peter V. Foukal, pp. 480. ISBN 3-527-40374-4. Wiley-VCH , April 2004., 2004.

Gary, G. A., R. L. Moore, M. J. Hagyard, and B. M. Haisch, Nonpotential features observed in the magnetic field of an active region, *ApJ*, *314*, 782–794, 1987.

Gorbachev, V. S., and B. V. Somov, Photospheric vortex flows as a cause for two-ribbon flares - A topological model, *Sol. Phys.*, *117*, 77–88, 1988.

Gorbachev, V. S., and B. V. Somov, Solar Flares of 1980NOV5 as the Result of Magnetic Reconnection at a Separator, *Soviet Astronomy*, *33*, 57–+, 1989.

Greene, J. M., Geometrical properties of three-dimensional reconnecting magnetic fields with nulls, *J. Geophys. Res.*, *93*, 8583–8590, 1988.

Handy, B. N., L. W. Acton, C. C. Kankelborg, C. J. Wolfson, D. J. Akin, M. E. Bruner, R. Caravalho, R. C. Catura, R. Chevalier, D. W. Duncan, C. G. Edwards, C. N. Feinstein, S. L. Freeland, F. M. Friedlaender, C. H. Hoffmann, N. E. Hurlburt, B. K. Jurcevich, N. L. Katz, G. A. Kelly, J. R. Lemen, M. Levay, R. W. Lindgren, D. P. Mathur, S. B.

Meyer, S. J. Morrison, M. D. Morrison, R. W. Nightingale, T. P. Pope, R. A. Rehse, C. J. Schrijver, R. A. Shine, L. Shing, K. T. Strong, T. D. Tarbell, A. M. Title, D. D. Torgerson, L. Golub, J. A. Bookbinder, D. Caldwell, P. N. Cheimets, W. N. Davis, E. E. Deluca, R. A. McMullen, H. P. Warren, D. Amato, R. Fisher, H. Maldonado, and C. Parkinson, The transition region and coronal explorer, *Sol. Phys.*, *187*, 229–260, 1999.

Henoux, J. C., and B. V. Somov, Generation and structure of the electric currents in a flaring activity complex, *Astronomy and Astrophysics*, *185*, 306–314, 1987.

Hirayama, T., Theoretical Model of Flares and Prominences. I: Evaporating Flare Model, *Sol. Phys.*, *34*, 323–+, 1974.

Högbom, J. A., Aperture Synthesis with a Non-Regular Distribution of Interferometer Baselines, *Astronomy and Astrophysics Supplement*, *15*, 417–+, 1974.

Hudson, H. S., Differential Emission-Measure Variations and the "Neupert Effect", in *Bulletin of the American Astronomical Society*, vol. 23 of *Bulletin of the American Astronomical Society*, pp. 1064–+, 1991.

Hurford, G. J., E. J. Schmahl, R. A. Schwartz, A. J. Conway, M. J. Aschwanden, A. Csillaghy, B. R. Dennis, C. Johns-Krull, S. Krucker, R. P. Lin, J. McTiernan, T. R. Metcalf, J. Sato, and D. M. Smith, The RHESSI Imaging Concept, *Sol. Phys.*, *210*, 61–86, 2002.

Kopp, R. A., and G. W. Pneuman, Magnetic reconnection in the corona and the loop prominence phenomenon, *Sol. Phys.*, *50*, 85–98, 1976.

Kosugi, T., S. Masuda, K. Makishima, M. Inda, T. Murakami, T. Dotani, Y. Ogawara, T. Sakao, K. Kai, and H. Nakajima, The hard X-ray telescope (HXT) for the Solar-A mission, *Sol. Phys.*, *136*, 17–36, 1991.

Krucker, S., M. D. Fivian, and R. P. Lin, Hard X-ray footpoint motions in solar flares: Comparing magnetic reconnection models with observations, *Advances in Space Research*, *35*, 1707–1711, 2005.

Lau, Y.-T., and J. M. Finn, Three-dimensional kinematic reconnection in the presence of field nulls and closed field lines, *ApJ*, *350*, 672–691, 1990.

Lee, J., P. T. Gallagher, D. E. Gary, G. M. Nita, G. S. Choe, S.-C. Bong, and H. S. Yun, Hα, Extreme-Ultraviolet, and Microwave Observations of the 2000 March 22 Solar Flare and Spontaneous Magnetic Reconnection, *ApJ*, *585*, 524–535, 2003.

Lin, R. P., B. R. Dennis, G. J. Hurford, D. M. Smith, A. Zehnder, P. R. Harvey, D. W. Curtis, D. Pankow, P. Turin, M. Bester, A. Csillaghy, M. Lewis, N. Madden, H. F. van Beek, M. Appleby, T. Raudorf, J. McTiernan, R. Ramaty, E. Schmahl, R. Schwartz, S. Krucker, R. Abiad, T. Quinn, P. Berg, M. Hashii, R. Sterling, R. Jackson, R. Pratt, R. D. Campbell, D. Malone, D. Landis, C. P. Barrington-Leigh, S. Slassi-Sennou, C. Cork, D. Clark,

D. Amato, L. Orwig, R. Boyle, I. S. Banks, K. Shirey, A. K. Tolbert, D. Zarro, F. Snow, K. Thomsen, R. Henneck, A. McHedlishvili, P. Ming, M. Fivian, J. Jordan, R. Wanner, J. Crubb, J. Preble, M. Matranga, A. Benz, H. Hudson, R. C. Canfield, G. D. Holman, C. Crannell, T. Kosugi, A. G. Emslie, N. Vilmer, J. C. Brown, C. Johns-Krull, M. Aschwanden, T. Metcalf, and A. Conway, The Reuven Ramaty High-Energy Solar Spectroscopic Imager (RHESSI), *Sol. Phys.*, *210*, 3–32, 2002.

Longcope, D. W., Topology and Current Ribbons: A Model for Current, Reconnection and Flaring in a Complex, Evolving Corona, *Sol. Phys.*, *169*, 91–121, 1996.

Longcope, D. W., Separator current sheets: generic features in minimum-energy magnetic fields subject to flux constraints, *Phys. Plasmas*, *8*, 5277, 2001.

Longcope, D. W., Topological Methods for the Analysis of Solar Magnetic Fields, *Living Reviews in Solar Physics*, *2*, 7–+, 2005.

Longcope, D. W., and C. Beveridge, A Quantitative, Topological Model of Reconnection and Flux Rope Formation in a Two-Ribbon Flare, *ApJ*, *in-press*, 2007.

Longcope, D. W., and I. Klapper, A General Theory of Connectivity and Current Sheets in Coronal Magnetic Fields Anchored to Discrete Sources, *ApJ*, *579*, 468–481, 2002.

Longcope, D. W., D. E. McKenzie, J. Cirtain, and J. Scott, Observations of Separator Reconnection to an Emerging Active Region, *ApJ*, *630*, 596–614, 2005.

Longcope, D. W., C. Beveridge, J. Qiu, B. Ravindra, G. Barnes, and S. Dasso, Modeling and Measuring the Flux Reconnected and Ejected by the Two-ribbon Flare on 7 November 2004, *Sol. Phys.*, *in-press*, 2007.

Mandrini, C. H., P. Demoulin, J. C. Henoux, and M. E. Machado, Evidence for the interaction of large scale magnetic structures in solar flares, *Astronomy and Astrophysics*, *250*, 541–547, 1991.

Metcalf, T. R., D. Alexander, H. S. Hudson, and D. W. Longcope, TRACE and Yohkoh Observations of a White-Light Flare, *ApJ*, *595*, 483–492, 2003.

Moon, Y.-J., H. S. Yun, G. Choi, Y. D. Park, and D. L. Mickey, Nonpotential Parameters of Solar Active Region AR 5747, *Journal of Korean Astronomical Society*, *33*, 47–55, 2000.

Neupert, W. M., Comparison of Solar X-Ray Line Emission with Microwave Emission during Flares, *ApJ Letters*, *153*, L59+, 1968.

Press, W. H., S. A. Teukolsky, W. T. Vetterling, and B. P. Flannery, *Numerical recipes in C. The art of scientific computing*, Cambridge: University Press, |c1992, 2nd ed., 1992.

Priest, E., and T. Forbes, *Magnetic Reconnection*, Magnetic Reconnection, by Eric Priest and Terry Forbes, pp. 612. ISBN 0521481791. Cambridge, UK: Cambridge University Press, June 2000., 2000.

Puetter, R. C., Pixon-based multiresolution image reconstruction and the quantification of picture information content, *International Journal of Imaging Systems and Technology*, *6*, 314–331, 1995.

Qiu, J., J. Lee, D. E. Gary, and H. Wang, Motion of Flare Footpoint Emission and Inferred Electric Field in Reconnecting Current Sheets, *ApJ*, *565*, 1335–1347, 2002.

Sakao, T., T. Kosugi, and S. Masuda, Energy Release and Particle Acceleration in Solar Flares with Respect to Flaring Magnetic Loops, in *ASSL Vol. 229: Observational Plasma Astrophysics : Five Years of YOHKOH and Beyond*, edited by T. Watanabe and T. Kosugi, pp. 273–+, 1998.

Scherrer, P. H., R. S. Bogart, R. I. Bush, J. T. Hoeksema, A. G. Kosovichev, J. Schou, W. Rosenberg, L. Springer, T. D. Tarbell, A. Title, C. J. Wolfson, I. Zayer, and MDI Engineering Team, The Solar Oscillations Investigation - Michelson Doppler Imager, *Sol. Phys.*, *162*, 129–188, 1995.

Somov, B. V., T. Kosugi, and T. Sakao, Collisionless Three-dimensional Reconnection in Impulsive Solar Flares, *ApJ*, *497*, 943–+, 1998.

Sturrock, P. A., A Model of Solar Flares, in *IAU Symp. 35: Structure and Development of Solar Active Regions*, edited by K. O. Kiepenheuer, pp. 471–+, 1968.

Temmer, M., A. M. Veronig, B. Vršnak, and C. Miklenic, Energy Release Rates along Hα Flare Ribbons and the Location of Hard X-Ray Sources, *ApJ*, *654*, 665–674, 2007.

Tian, L., J. Wang, and D. Wu, Non-Potentiality of the Magnetic Field Beneath the Eruptive Filament in the Bastille Event, *Sol. Phys.*, *209*, 375–389, 2002.

Titov, V. S., E. R. Priest, and P. Demoulin, Conditions for the appearance of ”bald patches” at the solar surface, *Astronomy and Astrophysics*, *276*, 564–+, 1993.

Titov, V. S., G. Hornig, and P. Démoulin, Theory of magnetic connectivity in the solar corona, *Journal of Geophysical Research (Space Physics)*, *107*, 3–1, 2002.

Titov, V. S., K. Galsgaard, and T. Neukirch, Magnetic Pinching of Hyperbolic Flux Tubes. I. Basic Estimations, *ApJ*, *582*, 1172–1189, 2003.

Wang, H., Y. Yan, T. Sakurai, and M. Zhang, Topology of Magnetic Field and Coronal Heating in Solar Active Regions - II. The Role of Quasi-Separatrix Layers, *Sol. Phys.*, *197*, 263–273, 2000.

Wang, J., Z. Shi, H. Wang, and Y. Lue, Flares and the Magnetic Nonpotentiality, *ApJ*, *456*, 861–+, 1996.

Wang, T., Y. Yan, J. Wang, H. Kurokawa, and K. Shibata, The Large-Scale Coronal Field Structure and Source Region Features for a Halo Coronal Mass Ejection, *ApJ*, *572*, 580–597, 2002.